Towards a circular nickel-plated steel (NPS) industry

A method to selectively dissolve nickel coatings from NPS in ammoniacal solutions.

By

Muawya Hindi

Master Thesis Report

Materials Science and Engineering Dep.

Delft University of Technology

Supervisors:

Dr. Aad Wittebrood, TATA Steel Nederland Technology BV.

Prof. Yongxiang Yang, Delft University of Technology

September 2024

Acknowledgments

I would like to express my deepest gratitude to the ones who have played a significant role in the successful completion of this thesis.

First and foremost, I would like to express my sincere thanks to my supervisor, Dr. Aad Wittebrood, for his invaluable guidance, continuous support, and encouragement throughout this research journey. His insightful advice and feedback have been crucial in shaping the direction and quality of this work, and I am deeply grateful for his patience and dedication.

I would also like to thank my academic supervisor, Prof. Yongxiang Yang, for his constant assistance and expertise. His constructive critiques, thoughtful input, and academic knowledge have been instrumental in navigating the various challenges encountered during this project.

A special thanks goes to Tata Steel Nederland Technology BV and its wonderful employees, who provided me with the resources, information, and support necessary to carry out this research. I am particularly thankful to Dr. Frank Schrama whose contributions were instrumental in identifying the thesis topic and introducing me to the company.

I would like to express my gratitude to Cleantron® for their support by providing waste Li-ion batteries, which were utilized for the purposes of this project.

Finally, I would like to thank my family for their unwavering support and encouragement during this research. Your belief in me has been a source of strength throughout this journey.

Thank you all.

Abstract

A patent pending ammonia-based hydrometallurgical method is developed to selectively leach nickel coatings from the Nickel-Plated Steel sheets (NPS). The leaching process starts with the removal of the passive nickel oxide film by $Na_2S_2O_3.5H_2O$ addition into the solution, followed by the dissolution of the metallic nickel. Leaching stops due to the passivation of the diffusion region between the coating and the steel. The experiments were conducted using two different ammoniacal systems, the NH_3-$(NH_4)_2S_2O_8$-$Na_2S_2O_3.5H_2O$ and the NH_3-$(NH_4)_2SO_4$-$Na_2S_2O_3.5H_2O$ system, resulting in leaching efficiencies of 98% and 91% respectively.

Table of contents

Table of Figures

1 Introduction

Nickel-plated steel (NPS) is an essential product used in various industries including automotive, aerospace, electronics, and household appliances. The process of nickel plating involves electroplating a thin layer of nickel onto the surface of steel. This process imparts a range of beneficial characteristics that make the product highly desirable for various industries; from enhancing aesthetics, to providing exceptional resistance against corrosion and wear. [1]

The NPS industry consumes 150,000 tonnes of "class 1" nickel annually (class 1 contains 99.8 % wt. nickel and above, class 2 contains less than 99.8 % wt. nickel). [1] [2] It is expected that nickel demand will increase by 60-70% in 2040 with respect to 2020, mainly due to the growing demand on electric vehicles (EVs). [3] The EVs are powered by batteries consisting of hundreds of Lithium-ion (Li-ion) battery cells, and each cell's housing is made of NPS. In addition, for a medium size electric car the cathode of the Li-ion battery cells contains 15-30 kg of pure nickel. [2] The growing demand for nickel is expected to exert significant pressure on the primary sources of nickel.

Since 2023, the European Commission has classified nickel as a critical element, specifically as a strategic raw material. [4] This indicates that the primary sources of nickel will be exhausted in the future due to the increasing demand. Moreover, the European Union (EU) has set a plan called the circular economy plan by which the EU is committed to decrease its dependence on natural resources and to improve the recovery of various materials from secondary resources (i.e., waste materials). The aim of this plan is to achieve economic growth and climate neutrality by 2050. [5] Therefore, efficient recycling of the steel and recovery of the nickel should be enhanced to achieve circularity and to release the pressure on the primary sources.

Currently, it is difficult to give an estimation about the amount of NPS waste. NPS waste includes several types of end-of-use NPS-containing products such as battery casings and factory offcuts. Some of the NPS waste is consumed by the stainless-steel and nickel alloys producers as a source of nickel and iron. [6] [3] While this recycling strategy may seem adequate, it does not fulfil the goal of achieving circularity for NPS. Class 1 nickel must be recovered and reused in the production of new NPS. Otherwise, it would need to be extracted from natural resources, which contradicts the principles of the circular economy.

Moreover, it is of importance to address the environmental and the social effects of nickel industry to understand the need for nickel recovery. The production of CO_2-eq (CO_2-eq indicates the equivalent environmental effect of all gas emissions) for nickel industry varies between 10-70 tonnes per 1 tonne (class 1) nickel depending on the ore type. [7] In addition, mining of nickel is responsible for deforestation, pollution of underground water, destruction of marine life, extinction of wildlife species. [8] [9] From a social perspective, mining has a dramatic impact on the social life, especially in the areas close to mining locations where the population may suffer from various diseases related to pollution and lack of safety measures in the working environment. [10] [11] [12]

Alongside the nickel industry, Steelmakers are also striving to achieve circularity and increase scrap consumption. Among these steelmakers are producers of NPS, who cannot recycle the NPS because of the nickel content. Nickel is categorized as a tramp element, in

addition to Cr, Cu, Sn, and Mo. Once these elements dissolve into the steel melt, they become difficult to remove and can adversely impact the steel's properties. [13]

The removal of nickel from NPS is not addressed in the literature but many studies investigated the recovery of nickel from different objects. The objects included nickel iron alloys, Li-ion battery cathodes, nickel coated magnets, and the laterite ores. In addition, some studies focus on the dissolution of nickel powders and pure nickel rotating discs in ammoniacal solution. The used methods in these studies were pyrometallurgical [14], electrochemical [15] [16], and hydrometallurgical. [17] [18] [19] [20] The hydrometallurgical methods especially the selective leaching with ammonia are potentially suitable to use for the purpose of this report. That is due to the availability of ammonia and ammonium salts on industrial scale, the method is less harmful to the environment, less toxic, and lower in energy consumption compared to the other methods.

In this report, the dissolution of nickel from NPS in different ammoniacal solutions will be investigated. In addition, the mechanism of the dissolution will be defined to setup a process to remove the nickel from the NPS. Moreover, the process parameters will be investigated to achieve optimum leaching results. Lastly, a brief feasibility study will be conducted to investigate the applicability of the process on industrial scale.

1.1 Literature research

The purpose of the literature research is to address the importance of achieving the circularity for the NPS industry, and to discuss the applicability of ammoniacal solutions to selectively remove the nickel coating from the NPS.

1.1.1 Relevance

This subsection introduces the core concepts related to steelmaking and electroplating processes for steel sheets, emphasizing the social, environmental, and political aspects of the NPS industry.

NPS production includes the casting of liquid steel into sheets, followed by nickel electroplating. The process starts at earlier stage with mining high-iron-content ores, processing them into sinter and pellets, and then using coke in a blast furnace to extract hot metal (HM). The HM undergoes desulfurization and is transformed into liquid steel in the Basic Oxygen Furnace (BOF). [21] The steel is further refined, cast, and rolled into sheets, preparing it for electroplating.

The preparation of steel sheets includes pickling to remove impurities and cold rolling for further thickness reduction. Plating might take place followed by annealing and temper rolling to produce battery casings and automotive applications as described in **Figure 1-1**. Alternatively, plating can take place after annealing and temper rolling, as shown in **Figure 1-2**. Plating after annealing provides bright surfaces and scratch resistant surfaces and is typically used for office equipment and decorative household products.

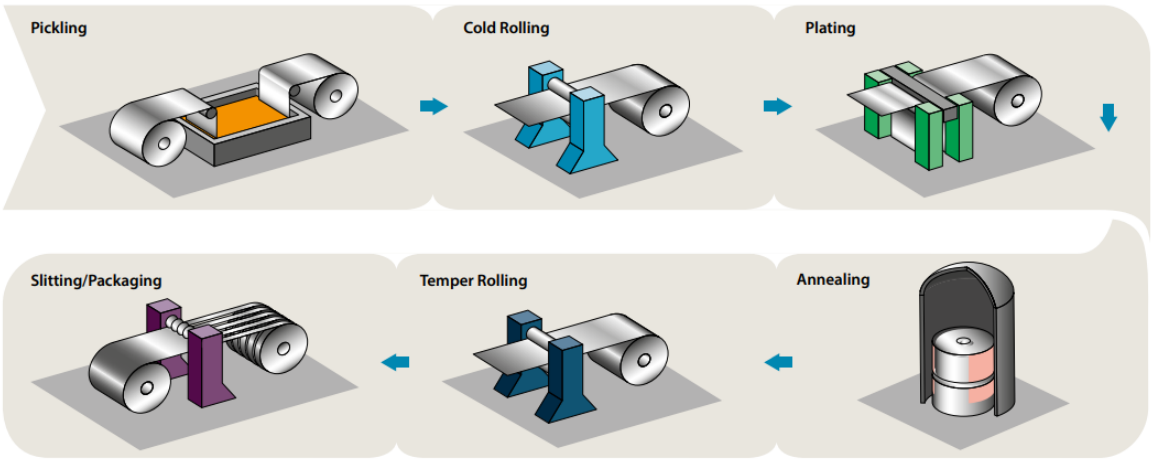

Figure 1-1. Plating before annealing and cold rolling. [22]

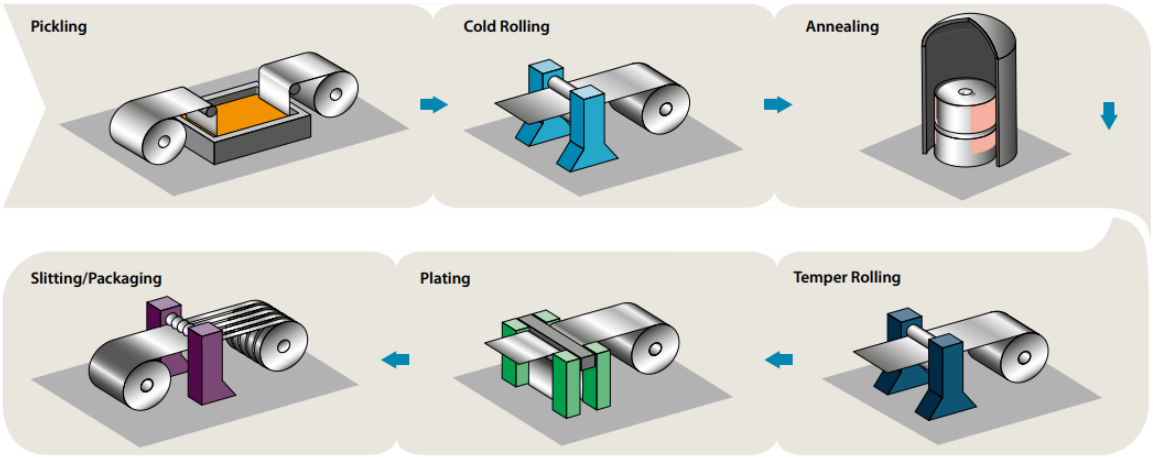

Figure 1-2. Plating after annealing and cold rolling. [23]

Nickel plating, first commercialized in the 19th century, involves coating steel for decorative and functional purposes, improving corrosion resistance, wear, and electrical conductivity. Electroplating occurs in an electrolytic cell with nickel anodes and an electrolyte containing nickel salts. Nickel ions transfer to the cathode, forming a nickel layer, while the anode dissolves to replenish the electrolyte. [1] [24]

Environmental, social, and political impact of nickel extraction from primary resources

The nickel industry significantly contributes to global CO_2 emissions, with variations depending on the methods used for extraction and processing. In 2019, nickel mining activities worldwide were responsible for approximately 120 million metric tons of CO_2-equivalent emissions. The emission intensity differs based on the type of nickel product being produced. For instance, ferronickel production generates around 45 kg of CO_2 for each kg of nickel content, while the production of nickel sulphate emits approximately 5.4 kg of CO_2 per kg produced. [7] Deforestation is one of the significant environmental challenges and an inevitable consequence of metals mining in the absence of proper environmental regulations. Nickel mining in Indonesia has been linked to the disappearance of rainforests [12], resulting in flooding, the destruction of ecosystems by placing numerous species at risk of extinction. [8] The destruction of marine life is often caused by the irresponsible mining activities near coastal areas, particularly through the disposal of waste containing nickel. [12] Flooding in the mining areas carry soil and pollutants into nearby water sources, contaminating both surface water and groundwater. [11]

The social impacts of nickel mining and production include health issues arising from water and air pollution, as well as exploitative practices such as child labour and human trafficking. Additionally, political instability can significantly impact the nickel industry, particularly in cases of conflicts between nickel-producing countries.
It is projected that by 2050, 80% of Namibia's population will face severe health issues due to pollution from the country's mining industries. [10] In some regions, children are forced to work in nickel mines to support their families, [9] [25] [26] [27] a practice that violates international standards. According to the International Labour Organization (ILO)

Convention No. 182, this form of child labour is among the worst and must be eliminated immediately.

Nickel mining and trade intertwines with the political conflicts in multiple ways. One significant aspect involves its utilization to fuel conflicts and connection with colonialism. [28] In 2017, the EU passed the conflict mineral regulation that call to stop importing the conflict minerals and to stop the EU smelters and refiners from using conflict minerals. [29] For instance, the conflict between Russia and Ukraine prompted the European Union to impose restrictions on economic ties with Russia. Consequently, this action led to a reduction in total nickel imports from Russia, declining from 42% of the EU's total nickel imports before the conflict to 29% by 2023. [4] [30]

All aspects discussed above support the instability of nickel. The environmental, and political impacts of nickel industry, address the importance of creating a more stable nickel supply through achieving the EU circular economy plan.

The availability of NPS scrap

The potential of NPS for recycling can be estimated by considering the end-of-use Li-ion and alkaline batteries, along with NPS from factory offcuts at TATA Steel Europe. In **Figure 1-3** we can see the global annual availability of Li-ion battery cells. It is remarked by an exponential growth and 750,000 tonnes will be available for recycling in 2025. [31] This number is expected to reach 4 million tonnes by 2040. [32]

In addition, The annual production of alkaline batteries is more than 10 billion cells, and the number is expected to increase significantly in the coming years. [33] In Europe, there are measures taken to achieve the circularity of the alkaline batteries, one of these measures is the collection of the waste batteries. Up to now, the collection target is about 45% of the end of use alkaline batteries is Europe. The remaining 55% ends up in the household waste. In other countries outside the European union, these measures are not existing and the alkaline batteries at end-of-life are landfilled [33]. In a small country like Lebanon for example, an annual amount of 53 million batteries is landfilled. [34] A proper waste collection strategy to achieve 100% collection of waste alkaline batteries is internationally required to enhance the recyclability of the NPS.

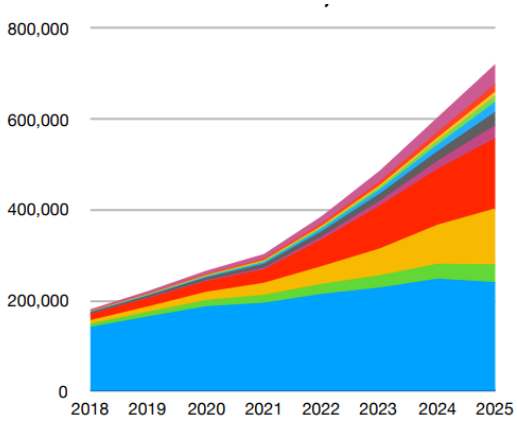

Figure 1-3. Lithium-ion batteries reaching end of life (global, tonnes). [31]

With respect to factory offcuts, there are no published data regarding their availability for recycling. The only reachable data can be obtained from TATA Steel Europe, a major NPS producer, because of their contributing to this work. In 2023 TATA Steel Europe has produced more than 6,110 tons of NPS offcuts. Figure 1-3 can give an indication to the growth in the production of NPS which probably will be exponential.

The availability of NPS for recycling will exponentially grow with time. That means there will be more class 1 nickel available to recover. The efficient recovery of this nickel will undoubtedly achieve the circularity of NPS industry.

1.1.2 Nickel removal by selective leaching in ammoniacal solutions

Selective leaching of nickel using ammoniacal solutions presents a promising approach for removing nickel from NPS. Numerous studies have demonstrated that nickel can be effectively removed from various materials, including laterite ores [20], end-of-life Li-ion battery cathodes [19], and nickel-iron alloys [35].

The process begins with the pretreatment of waste material to eliminate unwanted substances such as oils, binders, or other contaminants that could interfere with the leaching process. Depending on the nature of the waste material, pretreatment may involve thermal methods like roasting or chemical methods like solvent washing. Once pretreated, the material is immersed in an aerated leaching solution under carefully controlled conditions to maximize efficiency.

Several parameters play a critical role in determining the effectiveness of leaching. These include the composition and concentration of ammonia, the liquid-to-solid (L/S) ratio, the temperature, and the leaching time. By optimising these factors, the selective dissolution of nickel can be achieved efficiently.

The use of ammoniacal solutions for metal recovery dates to 1871, when they were first employed in copper mines to extract copper from mine waste. [36] Thirty years later, this method was expanded to recover copper, nickel, and cobalt from sulphide and oxidized ores. In 1921, Professor H.M. Caron of the Technische Hoogeschool te Delft [37], now known as Delft University of Technology, introduced an innovative technique, called the Caron process, utilizing ammoniacal solutions to extract nickel and cobalt from laterite ores. This process involved reduction roasting to convert nickel and cobalt oxides into their metallic forms, enabling efficient recovery.

The Caron process begins with drying and crushing the laterite ore to prepare it for further treatment. The ore is then subjected to reduction roasting in a rotary kiln or furnace at temperatures of approximately 700–800°C in a reducing atmosphere, typically achieved using reductants like coal or heavy oil. This step reduces nickel and cobalt oxides in the ore to their metallic forms while leaving iron oxides largely unaffected. [38]

Following reduction, the roasted ore undergoes ammonia leaching at elevated temperatures and pressures. In this step, ammonium carbonate and ammonia gas are used as leaching agents to selectively dissolve nickel and cobalt into solution, while iron remains in the solid residue. The leachate containing nickel and cobalt is subsequently processed to precipitate these metals as mixed carbonates or hydroxides, achieved by pH adjustment and the addition

of reagents such as ammonium hydroxide. The precipitates are then refined through further processing, such as smelting, to yield pure nickel and cobalt metals or salts.

Ammonia has excellent solubility in water. It forms a strongly alkaline solution known as ammonium hydroxide (NH_4OH). It is an effective complexing agent for transition metals such as cadmium, copper, nickel, cobalt, silver, gold, mercury, zinc, palladium, platinum, and others. [39]The formation of ammine complexes enhances the solubility of these metals in aqueous ammonia solutions. On the other hand, the +2-oxidation state of many of these metals, including nickel, which has a maximum coordination number of six forms amine complexes quickly. A principle that is employed in all the extraction and the recovery methods where nickel reacts with ammonia to form nickel hexamine. [40]

The reaction of the metallic nickel with ammonia is electrochemical by nature. [39] The cathodic reaction is represented by the oxidant which takes two electrons from the nickel and the nickel is consequently oxidised. On the other side, the anodic reaction is represented by the Ni giving off two electrons, leading eventually to the formation of nickel ammines following reaction (1.1).

$$Ni + 1/2\ O_2 + (n-2)NH_3 + 2NH_4^+ \rightarrow Ni(NH_3)_n^{2+} + H_2O \qquad (1.1)$$

To better understand the thermodynamics of the reaction between nickel and ammonia, it is important to examine Pourbaix or Eh-pH diagram, shown in **Figure 1-4**. These diagrams show the stable regimes of nickel ions in both simple and complex forms, nickel metal, and various nickel oxides at 1 atm pressure. The diagram illustrates that the formation of nickel amine complexes is more thermodynamically favourable at 298K than at 323K. the diagram at 298K shows that $Ni(NH_3)_6^{2+}$ is stable at pH between 10-11, and $Ni(NH_3)_5^{2+}$ is stable in the pH range of approximately 8-10.

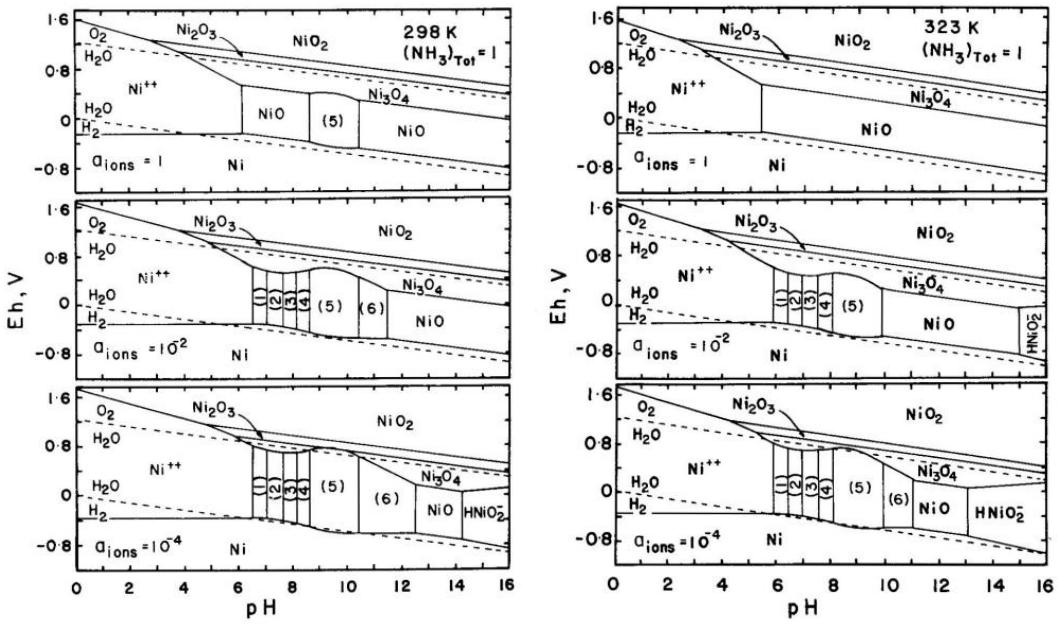

Figure 1-4 Eh-pH diagram for system at 298 (K) left, and at 325 (K) right.

The kinetics of nickel dissolution are discussed in several studies. All these focused mainly on the effect of the leaching parameters on the leaching efficiency. The parameters were the temperature, the concentration of NH_3, the liquid-solid ratio (L/S ratio), the concentration of

the ammonium salt, the concentration of the oxygenator, and other parameters related to the chemical nature of the studied material.

The low-grade nickelferous laterite ore are consisting of approximately 1.2 wt.% nickel and 45 wt.% iron. Both nickel and iron exist in the laterite ores as metal oxides. It is essential to carbothermal reduce the nickel oxide to its metallic form to ensure dissolution in ammonia. [41] Therefore, carbothermal reduction roasting is usually carried out to reduce nickel and iron oxides into ferronickel. [42]
The behaviour of iron is of importance here since both iron and nickel exist in their metallic states in both NPS, and the laterite ores after reduction roasting. It is found that iron does react with ammonia, following reaction 1.2, but the product of this reaction is not stable. Consequently, iron amine forms iron hydroxides, following reaction 1.3, in the solution and precipitates as a form of brownish powder.

$$Fe + ½\ O_2 + (n\text{-}2)NH_3 + (NH_4)_2CO_3 \rightarrow [Fe(NH_3)_n]CO_3 + H_2O \quad (1.2)$$

$$4[Fe(NH_3)_n]CO_3 + 10H_2O + O_2 \rightarrow 4Fe(OH)_3 + 4(n\text{-}2)NH_3 + 4(NH_4)_2CO_3 \quad (1.3)$$

The effect of Fe content on Ni leaching by ammonia was investigated in an earlier study. [35] The study included the preparation of three powdered Ni-Fe alloys with Ni content between 6.7 wt.%, 35 wt.% and 67 wt.% to stimulate the extraction of Ni from the laterite ores, as shown in **Table 1-1**.

Table 1-1 characterisation of the samples used by Jandova. [35]

Samples	Ni wt.%	Structure
1	67	α-Fe-Ni (BCC)
2	35	γ-Fe-Ni (FCC) with 50 wt.% of Ni and α-Fe-Ni (BCC) with 1-3 wt.% of Ni γ/α =3/1
3	5.2	γ-Fe-Ni (FCC)

The leaching solution consisted of 1.9 (kmol/m^3) NH_3 and 1.4 (kmol/m^3) $(NH_4)_2CO_3$ with pH of 10.4. The experiments were carried out at 40 ˚C with duration of 6 h. The liquid-solid weight ratio was 100-500:1 which changes depending on Ni content. Aeration of the solution took place upon starting the solution. The concentration of nickel in ammonia has shown rapid increase in the first 150 min and the dissolution of nickel in the solution increased with the increase of nickel content in the metallic powder, see **Figure 1-5**. Therefore, it is expected that if the same experiment is carried out on a NPS sample, dissolution of nickel in the ammoniacal solution is expected.

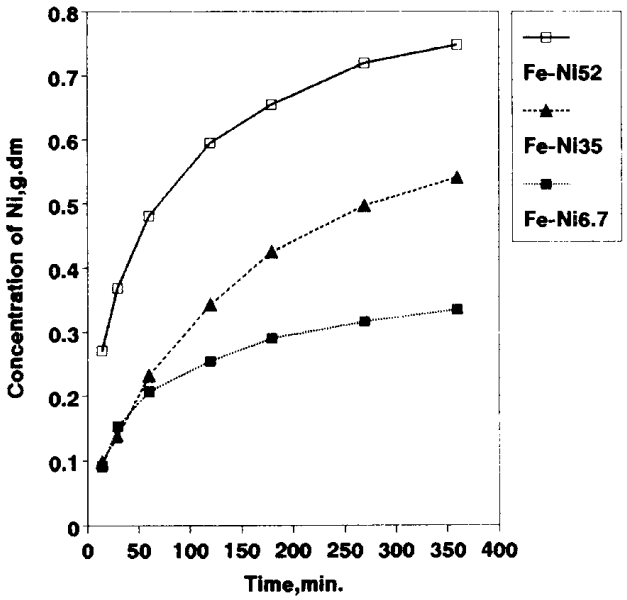

Figure 1-5 Nickel dissolution from the samples in Table 1-4 as a function of time.

Although the behaviour of iron in the solution was not studied by Jandova, he concluded that the dissolution rate is higher when the nickel content is high enough to form the γ phase in the alloy, in other words, the less iron in the alloy the higher the dissolution rate. This information is valuable because iron and nickel diffuse between each other in the NPS due to the annealing after nickel plating.

The recovery of Ni and other valuable element from Li-ion battery cathode material was also investigated intensively according to the literature. The nickel-containing cathodic material consists generally of crystals in the form of $LiNi_xCo_yMn_{1-x-y}O_2$. Many ammonia leaching systems were used under different leaching conditions to optimize leaching efficiency. Li et al [43] used the system NH_4OH-NH_4HCO_3-H_2O_2 to selectively leach Ni and Co from the spent cathode material. The process included reductive roasting of the cathodic material at 800^{o}C for 8 hours in the inert argon gas environment. The purpose of reduction roasting is to destroy the crystal structure of the cathodic material and to reduce the nickel to its metallic form. Then H_2O_2 is used in the solution to provide it with oxygen. The leaching efficiency was 99.65% for Ni at optimum leaching parameters of (3M) NH_4HCO_3, 5 vol% H_2O_2, leaching temperature of 80 °C, S/L ratio is 20g/litre, and leaching duration of 60 minutes.

Electrochemical studies on the nickel dissolution into ammonia-ammonium carbonate solutions have shown that nickel dissolution is difficult without the addition of thiosulfate. [44] The presence of thiosulfate enhances the dissolution by forming a mixed sulphide layer with nickel and cobalt. This reaction, facilitated at potentials below -0.9 V, is described as:

$$Ni(NH3)_5^{2+} + S_2O_3^{2-} + 6H^+ + 8e^- \rightarrow NiS + 10NH_3 + 3H_2O \qquad (1.4)$$

These sulphide layers enhance leaching efficiency by preventing the complete passivation of the alloy surface, allowing sustained metal dissolution.

2 Methodology

The methodology for this study involved the preparation and analysis of nickel-plated steel (NPS) samples, as well as the evaluation of leaching efficiency. More than 200 Samples were provided by TATA Steel Nederland and cut into size of 50×50 mm^2, cleaned with acetone, and dried with clean paper. The amount of nickel on the surface of each sample was measured using a Handheld X-Ray Fluorescence (XRF) device, OXFORD® X-MET 8000 optimum, with measurements taken at four points per side as shown in **Figure 2-1**. The initial weight of each sample was recorded before subjecting it to leaching experiments. After leaching, the same measurements were repeated.

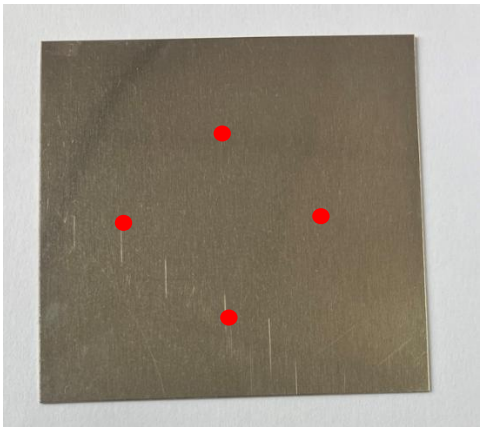

Figure 2-1 A typical NPS sample with a size of 50×50 mm^2. The four red dots on the sample represent the positions where the XRF analysis was performed.

Glow Discharge Optical Emission Spectroscopy (GDOES) analysis of the surface of a representative NPS sample was provided by TATA Steel. Each sample has two sides with different thicknesses. **Figure 2-2** shows the GDOES analysis where the thicker side, referred to as side 1, has a nominal thickness of 4 µm, while the thinner side, referred to as side 2, has a nominal thickness of 1µm. This specific type of NPS is referred to as 2A sample in this report. The figure also shows the iron content through the thickness of the nickel coating which start to increase from about 0 wt% at the surface to about 100 wt% at depth of 6.7 µm at side 1 and 2.5 µm at side 2.

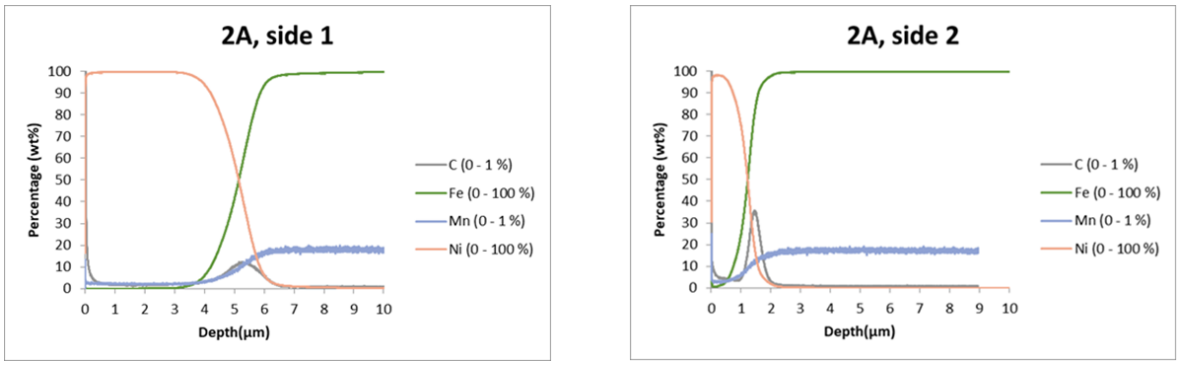

Figure 2-2 GDOES analysis for the NPS (type 2A) sample shows the nickel content through the thickness of the sample on side 1 on the left and side 2 on the right.

To study the effect of varying iron content across the thickness of the nickel coating, a different set of NPS samples, referred to as type 1A for convenience, was utilized. These samples underwent an alternative heat treatment process, resulting in increased diffusion between iron and nickel. The impact of this variation in nickel and iron content near the surface can be observed in **Figure 2-3**, particularly in the region between the steel sheet and the nickel coating. This region is notably wider in the 1A samples compared to the 2A samples.

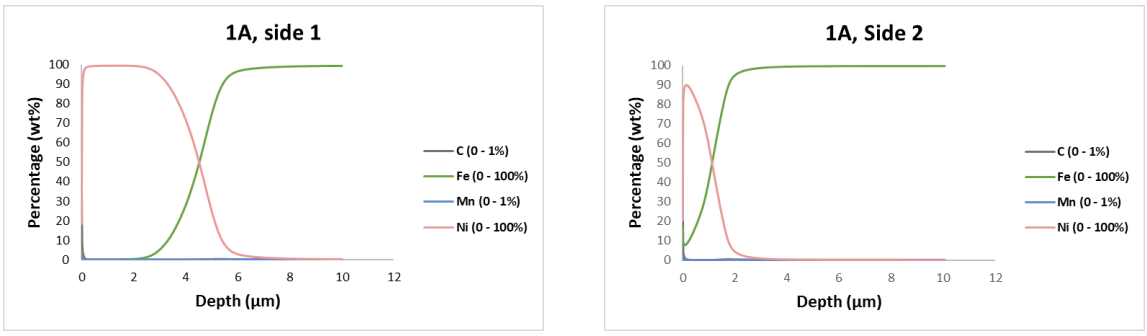

Figure 2-3 GDOES analysis for the NPS (type 1A) sample shows the nickel content through the thickness of the sample on side 1 on the left and side 2 on the right.

The leaching solutions were prepared by diluting analytical-grade ammonium hydroxide (NH_4OH) with distilled water to the desired concentration in a 300 ml beaker, followed by dissolving sodium thiosulfate pentahydrate $Na_2S_2O_3.5H_2O$ into the solution. Ammonium sulphide $(NH_4)_2SO_4$ or ammonium persulfate $(NH_4)_2S_2O_8$ was then added. Subsequently, the solution was aerated by air blowing to supply the necessary oxygen. Alternatively, hydrogen peroxide (H_2O_2) was used as an alternative oxygen source. The leaching experiments examined the effect of substituting oxygen with $(NH_4)_2S_2O_8$ as the oxidant. In this context, $(NH_4)_2S_2O_8$ served a dual role as both the ammonium salt and the oxidant.

The leaching efficiency was calculated based on the change on XRF measurements, in g/m^2, for each sample following equation (E2.1) where Xrf_{before} is the XRF measurement before leaching and xrf_{after} is the XRF measurement after leaching.

$$\text{Leaching efficiency} = \frac{Xrf_{before} - xrf_{after}}{Xrf_{before}} 100\% \qquad \text{E2.1}$$

The XRF results at different leaching times were validated by measuring the change in the weight of the samples and the nickel content in the solution at the same leaching times. To investigate the nickel content in the solution, Inductively Coupled Plasma Optical Emission Spectroscopy (ICP-OES) analysis of the leaching solutions was utilised

Post-leaching, the samples were analysed by X-ray photoelectron spectroscopy (XPS) to examine the chemical states on the surfaces. Scanning electron microscopy (SEM) and energy-dispersive X-ray spectroscopy (EDX) were used to investigate the surface morphology and elemental composition. For depth profiling of elemental distribution, glow discharge optical emission spectroscopy (GDOES) was applied.

In addition, pure copper, pure cobalt, and zinc plated steel (ZPS) samples with size of 50×50 mm^2 were used to investigate the ability of ammoniacal solutions to dissolve Co, Zn, and

copper. Moreover, two waste Li-ion batteries were dismantled and their casing were subjected to leaching under two different leaching conditions as will be later explained in the results and discussion section.

3 Results and discussion

The leaching experiments revealed that $Na_2S_2O_3.5H_2O$ plays a crucial role in initiating the leaching process by removing the naturally formed nickel oxide film as will be discussed in the leaching mechanism section. Additionally, it is essential to add the oxidant to the solution only after immersing the sample.

Through extensive trial-and-error testing, two leaching solutions were developed: one consisting of NH_3-$Na_2S_2O_3.5H_2O$-$(NH_4)_2SO_4$-H_2O_2 and the other containing NH_3-$Na_2S_2O_3.5H_2O$-$(NH_4)_2S_2O_8$. Both solutions were optimized to selectively remove nickel coatings and achieve maximum leaching efficiency. When applied to waste Li-ion battery casings, the solutions containing $(NH_4)_2S_2O_8$ demonstrated superior leaching efficiency compared to the solutions containing $(NH_4)_2SO_4$. Furthermore, the persulfate solution effectively dissolved copper, cobalt, and zinc from the ZPS.

3.1 The leaching mechanism

The experiments to remove nickel from the NPS samples were not successful in the absence of $Na_2S_2O_3.5H_2O$. That is possibly due to the naturally formed passive layer that prevents the ammoniacal solution from reaching the metallic nickel. **Figure 3-1** shows the SEM and the elemental mapping of the surface of the NPS sample before leaching and indicates high intensity of nickel and oxygen at the surface of the sample which could be related to the presence of a nickel oxide layer on the surface. This agrees with the GDOES results in **Appendix B** that shows more than 95 at% nickel and around 10 at% of oxygen content on the surface of the reference sample, which represents the non-leached sample.

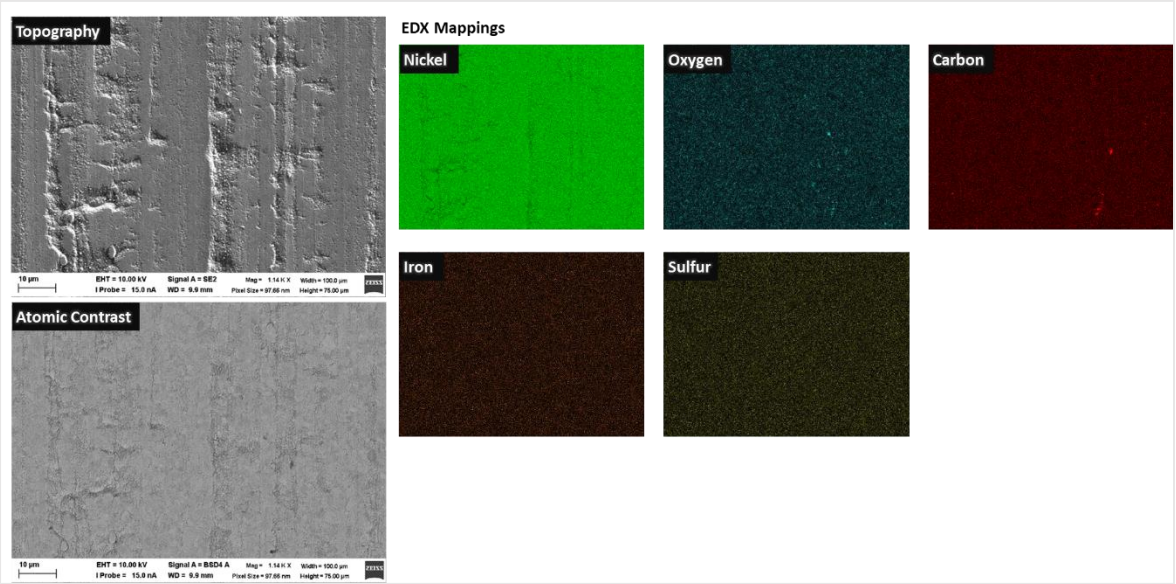

Figure 3-1 SEM and elemental mapping of the NPS sample prior to leaching.

The preliminary experiments including $Na_2S_2O_3.5H_2O$ addition in the solution resulted in rapid dissolution of nickel. The nickel layers on the NPS samples were dissolved within less than 15 min with leaching efficiency higher than 90%. The observed effect of $Na_2S_2O_3.5H_2O$ is supported by many studies on the dissolution of nickel, the corrosion of nickel alloys [44] [45], and the corrosion of stainless steels [46]. Apparently, the $Na_2S_2O_3.5H_2O$ reacts with the

passive layer which consists possibly of nickel (II) oxide (NiO) and produces nickel (II) sulphide following reaction (3.1).

$$NiO + S_2O_3^{2-} \rightarrow NiS + SO_4^{2-} \quad (3.1)$$

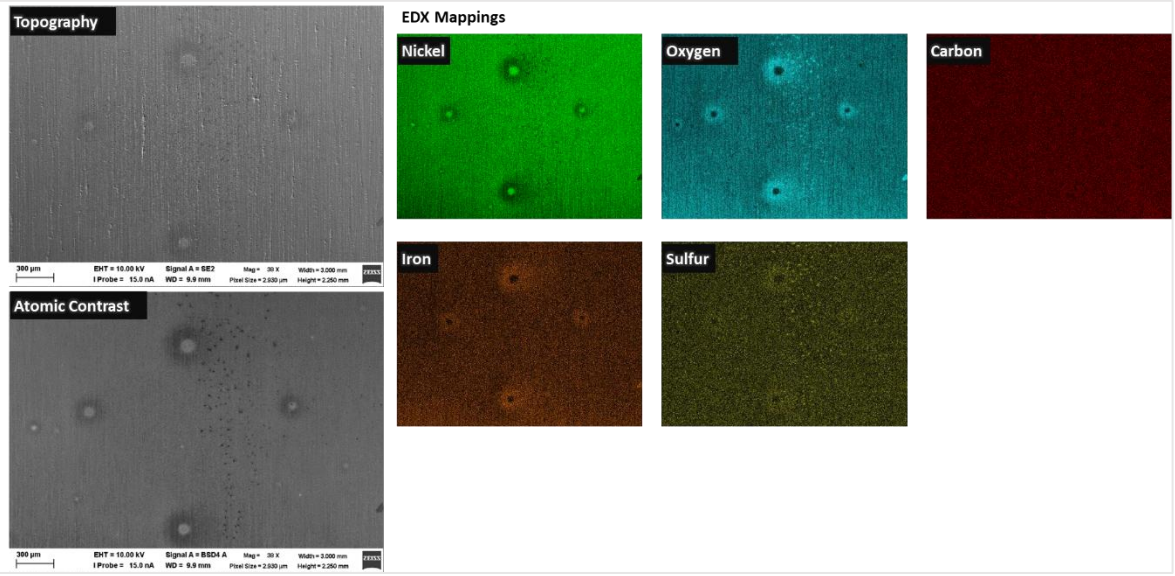

Figure 3-2 SEM and EDX elemental mapping of NPS type 2A sample after 20 seconds leaching in NH_3-$(NH_4)_2SO_4$- $Na_2S_2O_3.5H_2O$ -H_2O_2 System.

Figure 3-2 gives valuable information about the mechanism how the passive layer decomposes. At the early stages of the leaching process, the passive film is locally removed at many locations at the surface of the sample. In these locations, the circular spots, only nickel can be observed with clear absence of oxygen implying that the passive layer is removed.

Once the metallic nickel beneath the passive film is exposed to the ammoniacal solution, the oxidant, for example $S_2O_8^{2-}$, reacts with the metallic nickel as shown in the reaction (3.2). Then nickel forms nickel hexamine following reaction (3.3)

$$Ni + S_2O_8^{2-} \rightarrow Ni^{2+} + 2SO_4^{2-} \quad (3.2)$$

$$Ni^{2+} + 6NH_3 \rightarrow Ni(NH_3)_6^{2+} \quad (3.3)$$

The ammoniacal system continues with leaching until it reaches a point on the diffusion layer where iron or nickel passivates and leaching stops. More about the passivation at the end of the process will be discussed in section 3.3.

It is important to mention that each system appears to work only under a specific order of chemicals addition to the solution. The reason behind this behaviour will be explained in section 2. For the system NH_3-$Na_2S_2O_3.5H_2O$ -$(NH_4)_2S_2O_8$ the order starts with the addition of NH_3 and $Na_2S_2O_3.5H_2O$, then the NPS sample should be immersed to the solution, followed by the addition of $(NH_4)_2S_2O_8$.

For the system NH_3-$Na_2S_2O_3.5H_2O$ -$(NH_4)_2SO_4$-H_2O_2, the leaching process should have the following order: preparing the desired NH_3 concentration, $Na_2S_2O_3.5H_2O$ addition, then the immersion of the NPS sample followed by the addition of H_2O_2.

3.2 The importance of maintaining a specific experimental procedure.

As discussed in the previous section, the preparation of the solution should follow a specific order before starting the leaching experiment. The addition of the oxidant before the immersion of the sample will not result in leaching. A behaviour that requires more work to explain. On the other hand, immersing the sample into the solution before the oxidant will give the chance for the $Na_2S_2O_3.5H_2O$ to remove the passive film, then when the oxidant is added, leaching will start due to the oxidation of the metallic nickel and consequently the dissolution in the ammoniacal solution.

Once the leaching process is started, the sample should not be removed from the solution and exposed to air. The exposure will passivate the sample rapidly and will prevent resuming the leaching process if the sample is re-immersed. The partially leached sample in **Figure 3-3** shows a rainbow effect on the surface which resulted from the reflection of light through a passive layer with different thicknesses. These passive layers are difficult to remove by the ammoniacal solution and therefore, leaching is difficult to be resumed.

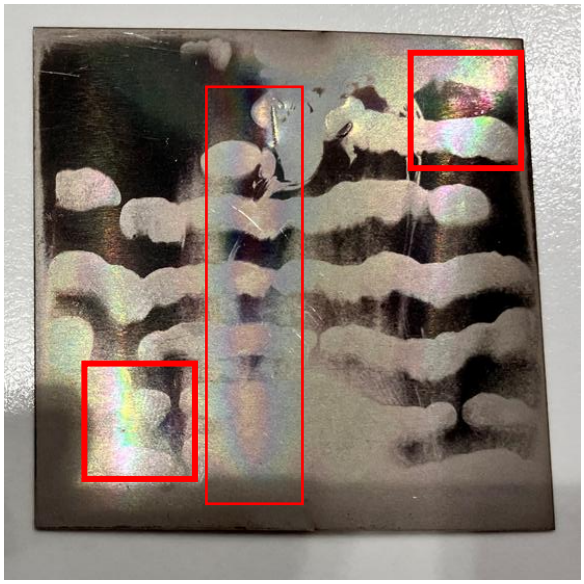

Figure 3-3 NPS sample leached for 30 seconds showing the rainbow effect.

3.3 The passivation of iron-nickel diffusion region

The preliminary experiments on the NPS samples showed lower leaching efficiency of side 2 compared with side1. The iron content through the nickel thickness is higher for side 2 compared with side 1 and therefore, it is assumed that the iron content influences the passivation of the sample.

For further experimental investigations on whether the passivation is linked to the iron content or not, two types of NPS, the 2A and the 1A type were subjected to leaching under similar conditions.

The leaching results, shown in **Figure 3-4**, indicate that the total leaching efficiencies for 1A and 2A are 80.1% and 91.6% respectively. The leaching results support the assumption that higher iron content will lead to lower leaching efficiency. The same conclusion can be found

in another study related to the leaching behaviour of iron-nickel alloys in the ammoniacal solutions. [35]

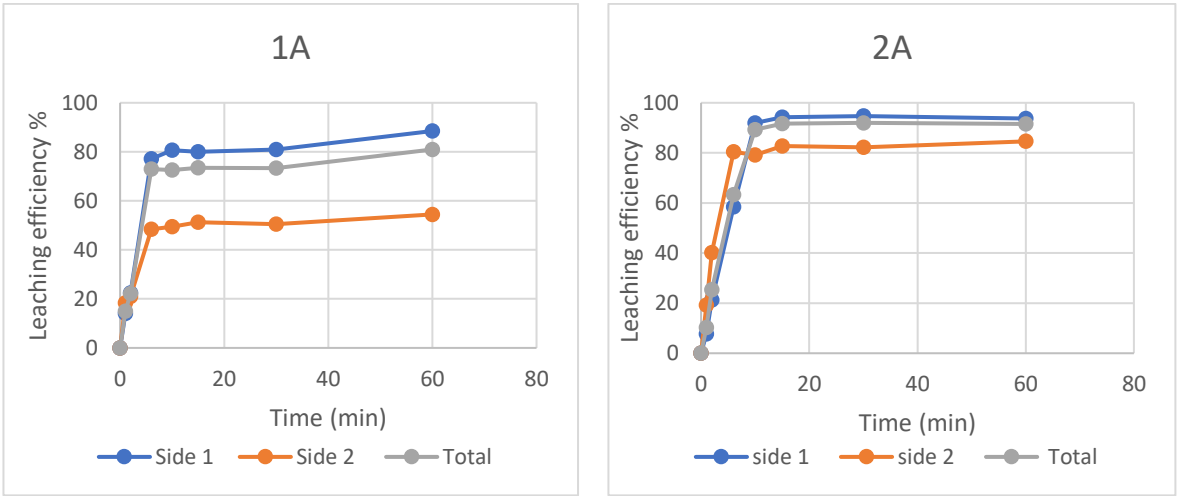

Figure 3-4 The leaching efficiency curves for two types of NPS. 1A has more iron content due to larger diffusion area.

However, the SEM and EDX results in **Figure 3-5** for the 2A sample after leaching show high levels nickel, oxygen, and iron. Therefore, the formation of nickel oxide and/or iron oxide is suggested as a reason for passivation. The XPS scan for the passive layer in **Figure 3-6** shows that the surface is rich of iron, and oxygen which agrees with the EDX mapping.

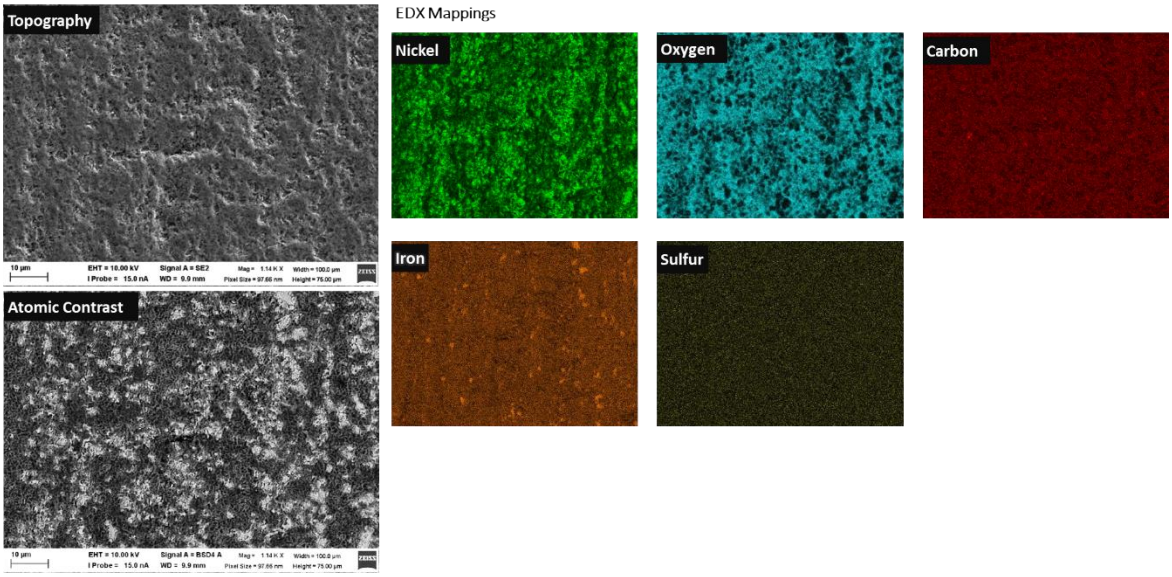

Figure 3-5 SEM and EDX elemental mapping for the 2A NPS sample after 7 min leaching in the NH_3-$(NH_4)_2SO_4$- $Na_2S_2O_3.5H_2O$ -H_2O_2 System

The XPS scan shows high intensity of oxygen at around 530 eV, carbon at 380 eV, and iron at 700 eV and above. These values are very close to what is reported in another study [47]

that investigated the passivation of iron in ammoniacal solutions and concluded that these values are related to the formation of Fe_3O_4.

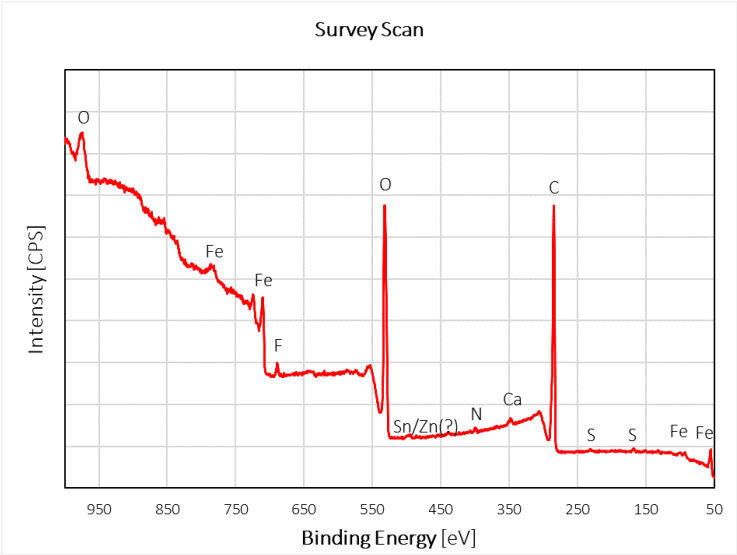

Figure 3-6 XPS analysis for the surface of the NPS type 2A sample leached for 7 min (420 sec) in the NH_3-$(NH_4)_2SO_4$- $Na_2S_2O_3.5H_2O$ -H_2O_2 System

The presence of nickel in the EDX mapping and its absence in the XPS results is surprising. That could be due to the resolution limit of both techniques. The EDX has usually a resolution depth of ≤ 1 µm while it is in the order of few nanometres for the XPS. More details about the surface can be obtained by the GDOES analysis for the region around the surface. **Figure 3-7** shows the results of the leached 2A sample in a NH_3-$(NH_4)_2SO_4$-$Na_2S_2O_3.5H_2O$-H_2O_2. On side 2 the results show that the surface around 0 µm depth consists of 77 wt.% oxygen, 12 wt.% carbon, 5 wt.% iron, and less than 1 wt.% nickel. The nickel content increases at more depth to levels higher than 50 wt% at both sides and starts to decrease again at 0.13 µm depth. This indicates that most of the non-leached nickel is located beneath the surface and probably covered by the Fe_3O_4 layer. The results for side 1 in the same figure show lower iron, carbon, and oxygen content on the surface, and similar nickel content near the surface.

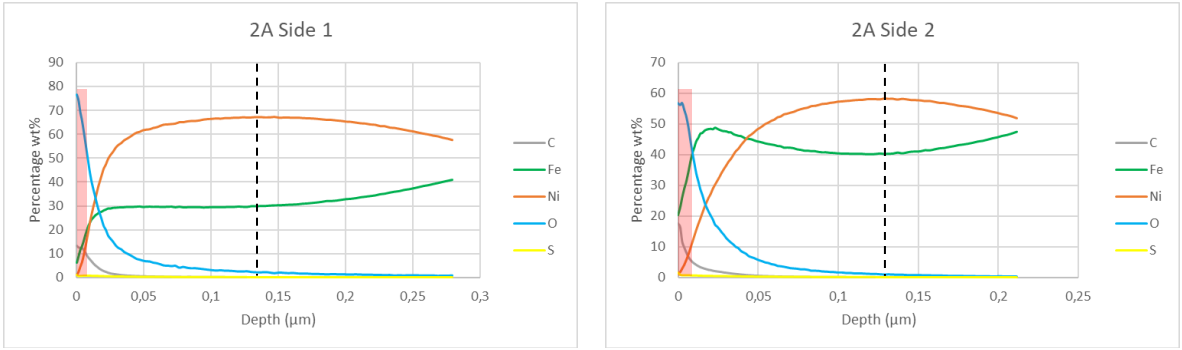

Figure 3-7 GDOES analysis for the 2A sample leached for 7 min (420 sec) in the NH_3-$(NH_4)_2SO_4$- $Na_2S_2O_3.5H_2O$ -H_2O_2 System

The GDOES analysis reveals information that helps to approximate the thickness of the passive layer and at what alloy composition the leaching process stops. Back to Figure 3-7**,**

assuming that the point of intersection between iron and oxygen represents the end of the passive film, then the thickness of the passive film will be represented by the shaded regions in the figure. The thickness is approximately 0.015 µm for both sides. Another assumption can be made regarding the nickel-iron ratio at which leaching stops. Supposing that leaching stops at the highest nickel content from the figure, marked by the dashed line. Leaching stops on side 1 at 68 wt.% nickel and 30 wt.% iron. While on side 2 it stops at 59 wt.% nickel and 40 wt.%. iron.

Following the same assumption, the passive layer formation analysis by GDOES in **Figure 3-8** reveals different results when the sample is leached in NH_3-$(NH_4)_2S_2O_8$-$Na_2S_2O_3.5H_2O$ system. The point when leaching stops for side 1 is 46 wt.% nickel and 46 wt.% iron. While on side 2, leaching stops at 46wt% nickel and 47wt% iron. Near 0 µm depth, side 2 shows different composition than it on side 1. Side 2 contains more iron content than oxygen and higher nickel content (~ 5 wt.%) which might be related to a different passive film type that needs to be identified by XPS analysis.

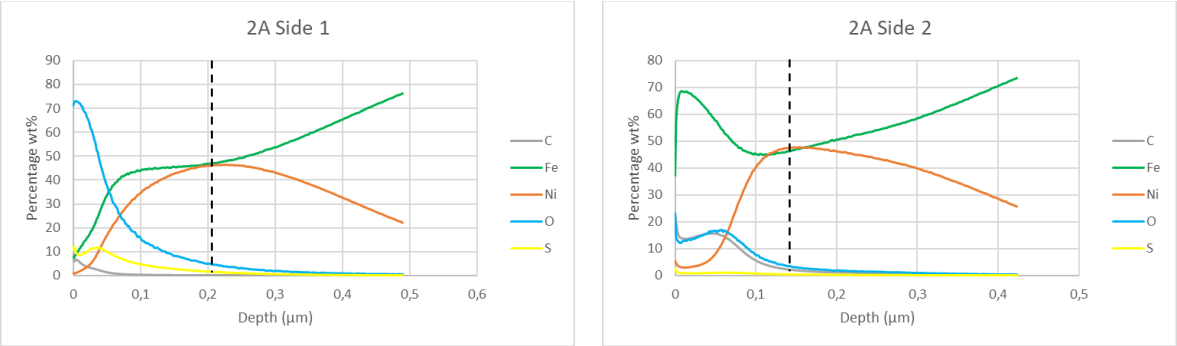

Figure 3-8 GDOES analysis for the 2A sample leached for 7 min (420 sec) in the NH_3-$(NH_4)_2S_2O_8$- $Na_2S_2O_3.5H_2O$ System.

The differences in Figure 3-7 and Figure 3-8 show that leaching stops at different points depending on the ammoniacal system used and the iron content through the nickel thickness. Changing the leaching parameters like the temperature, chemicals concentration and leaching time might result in a change on the point where leaching stops. In all cases, based on the original GDOES graph in **Figure 3-9** it can be concluded that most of the nickel coating can be removed and part of the nickel in the diffusion region can be selectively leached.

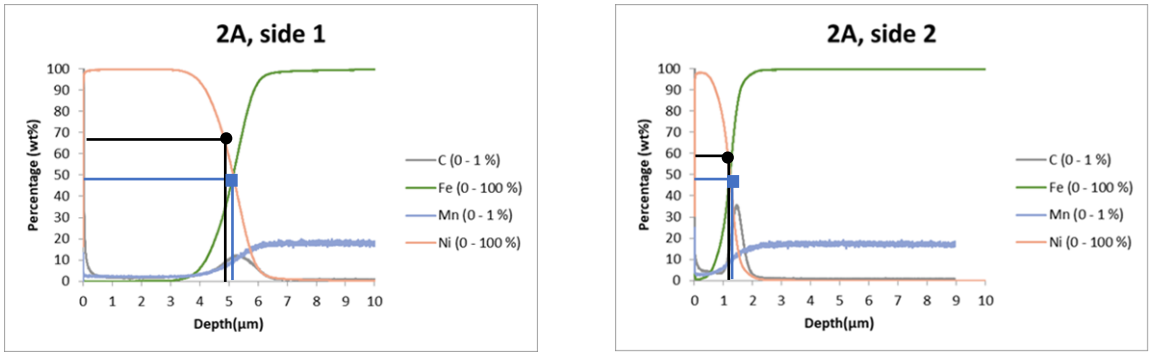

Figure 3-9 the points where leaching stops depending on the ammoniacal system. The black dots are related to the NH_3-$(NH_4)_2S_2O_8$- $Na_2S_2O_3.5H_2O$ System. The blue squares are related to the NH_3-$(NH_4)_2SO_4$- $Na_2S_2O_3.5H_2O$-H_2O_2 System

3.4 ICP analysis for the leaching solution

In **Figure 3-10**, the concentration of the dissolved nickel in the solution is plotted against leaching time. The concentration is obtained by three methods, the first method is measuring the lost nickel content from the sample by calculating the difference in the XRF measurements before and after leaching. The second method is by measuring the samples' weight difference before and after leaching. While the third is by performing the ICP analysis for the pregnant solution.

The weight loss measurements are higher than the ICP results for most of the time steps. The difference becomes noticeable after 3 minutes of leaching. That is due to lower accuracy of the balance compared to the ICP.

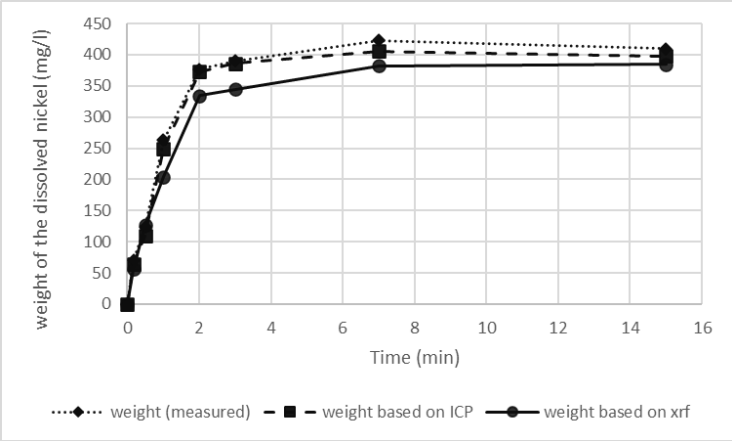

Figure 3-10 the amount of the dissolved nickel as measured by ICP and calculated by weight analysis and XRF analysis of the NPS samples. The experiment was carried out in a 300 ml solution with [NH3] =1.5 M, T = 40°C, $[Na_2S_2O_3.5H_2O]$ = 0.40 g/l, time = 7min, and H_2O_2 35% solution = 10 ml/l.

The values based on the XRF measurements are lower than the ICP results because the 4 points of XRF measurements taken from the sample do not accurately represent the whole sample's surface after leaching. **Figure 3-11** shows the variations in the XRF measurements on the sample's surface after leaching for 3 minutes. The variation reached more than 10

g/m^2. which indicates that nickel is not evenly removed from the surface of the sample and more than 4 measurements are required for better comparison with the ICP results.

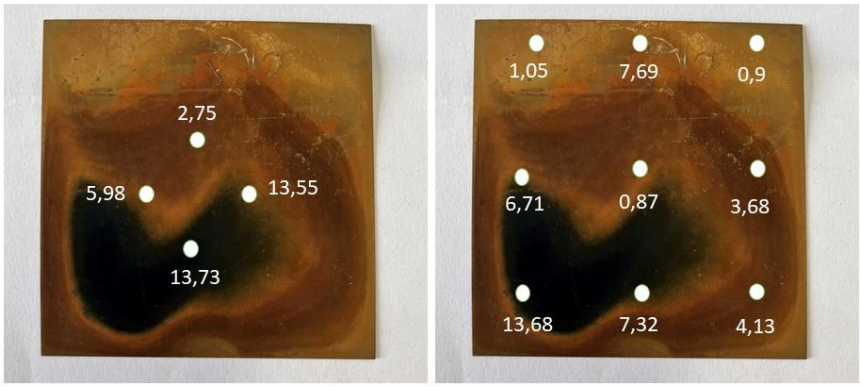

Figure 3-11 Side 2 of NPS sample leached for 3 minutes, on the right the XRF measurements taken for all the samples in this report the numbers are in g/m^2. On the right the XRF measurements taken for a comparison with ICP.

3.5 System NH_3-$(NH_4)_2S_2O_8$- $Na_2S_2O_3.5H_2O$

Understanding the kinetics of the leaching process is crucial for creating the required environment for the nickel recovery on industrial scale. The parameters that are of importance to discuss here are leaching time, leaching temperature, NH_3 concentration, $Na_2S_2O_3.5H_2O$ concentration, $(NH_4)_2S_2O_8$ concentration, and the Solid-to-Liquid S/L ratio. The result for each parameter is plotted against the leaching efficiency, and each point on the plot represents a different experiment with a new sample and a fresh solution.

Influence of time

Figure 3-12 shows a plateau like behaviour which starts at 7 minutes of leaching. The total leaching efficiency at 7 minutes is (87.4 ± 0.6) %. Moreover, the leaching efficiency for side 2 reaches the plateau at 2 minutes while side 1 reaches it at 7 minutes. This behaviour is expected because side 1 is four times thicker than side 2 and needs more time to be removed from the steel substrate. The optimum leaching efficiency of side 2 is (76.6 ± 0.6) % at 7 minutes, and for side 1 is (90.6 ± 0.6) % at the same leaching time. The variation in the leaching efficiency is related to the iron content as discussed earlier.

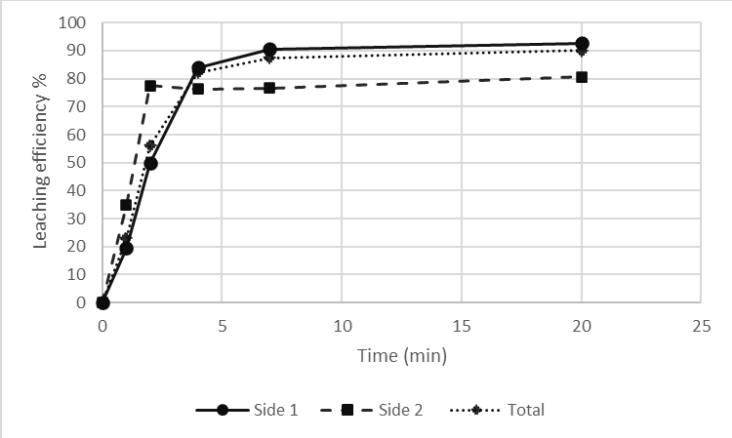

Figure 3-12 Leaching efficiency as a function of time. [NH_3] =2 M, [$(NH_4)_2S_2O_8$] = 33.3 g/l, [$Na_2S_2O_3.5H_2O$] = 6.7 g/l, and T= 20^oC.

The changes observed on the samples' appearance during the experiments are illustrated in **Figure 3-13**. At the start of leaching, a black colour appears due to the formation of pits on the surface, which is evident in the samples leached for 1 and 2 minutes. This black colour gradually fades over time. By the end of the experiment, marked by the beginning of the plateau observed in the figure at 7 minutes, the black colour has disappeared completely, and the surface has turned brown. This brown coloration is an indication the surface is completely passivated.

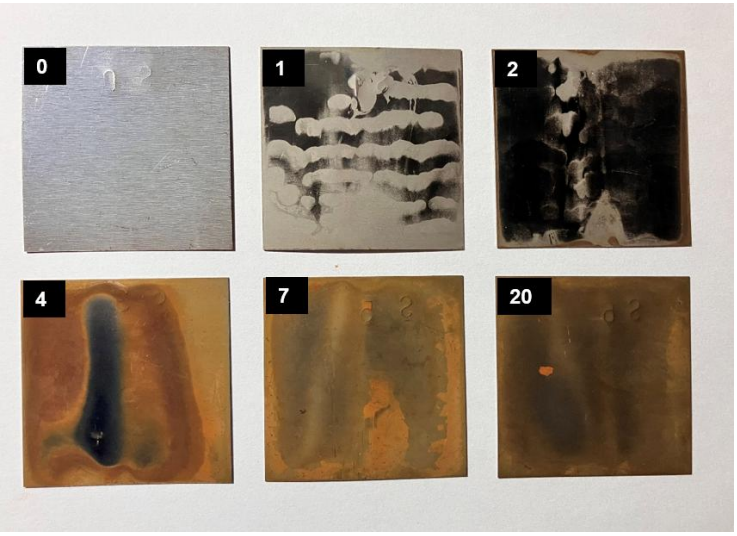

Figure 3-13 Leaching effect on the appearance of the NPS samples at different leaching times of 0, 1, 2, 4, 7, and 20 (min) as indicated on the samples.

Influence of temperature

It appears from **Figure 3-14** that the temperature has marginal effect on the leaching efficiency. The lowest total leaching efficiency is (87.4 ± 0.6)% and achieved at 20^oC, while the highest leaching efficiency is achieved at 50^oC which is 93.5%. The leaching efficiency at

80°C is less than that at 50°C, that is apparently due to the volatilisation of NH_3 that leads to decrease in ammonia concentration which in turns reduce the leaching efficiency.

Increasing the temperature of the solution is energy intensive especially when it becomes required on industrial scale. Avoiding heating of large volumes of ammoniacal solutions saves energy and prevents ammonia volatilisation. Therefore, in this experimental setup the optimum temperature will be 20°C.

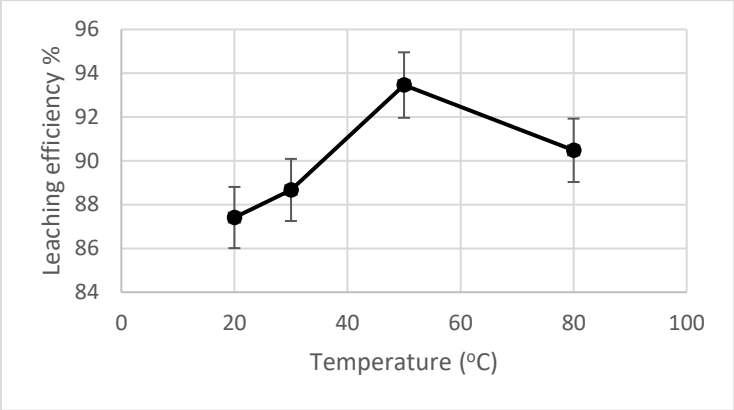

Figure 3-14 Temperature effect on the leaching efficiency. [$(NH_4)_2S_2O_8$] = 33.3 g/l, [NH_3] =2 M, [$Na_2S_2O_3.5H_2O$] = 6.7 g/l, and leaching time = 7 min.

Influence NH_3 concentration.

The experiments related to the variations in ammonia concentration show unexpected behaviour as can be seen in **Figure 3-15**. In ammonia-free solutions, the total leaching efficiency reaches 55.6%. Ammonia is required to permit the formation of nickel amine complexes. Apparently, the dissolution of $(NH_4)_2S_2O_8$ in water might provide the system with the required ammonia.

At ammonia concentrations of 0.5 and 1 M, leaching efficiency is 0%. Another 5 leaching experiments with the same ammonia concentrations were conducted and the leaching efficiency remained 0% for unknown reason. An electrochemical study to investigate the potential of the reaction and compare it with the Eh-pH diagram might provide a clarification.

The total leaching efficiency at 1.5 M and higher concentrations increased with the increase of ammonia concentration until it reached maximum of 97.5% at 5 M. At concentration of 13 M, the total leaching efficiency was 52.6%. The reason behind the drop is the decrease in the solution's temperature which reached 2°C during the experiment. Solutions with such high ammonia concentrations start to lose heat when the solution is exposed to the atmosphere due to evaporation. The evaporation of ammonia is endothermic and causes temperature drop. While the temperature remains low because there was no heat applied to maintain the solution's temperature at 20°C which eventually resulted in lower leaching efficiency.

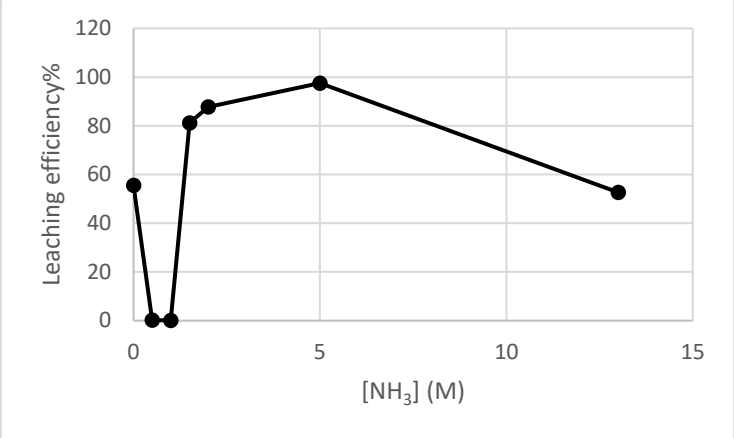

Figure 3-15 The effect of NH_3 concentration on the leaching efficiency. $[(NH_4)_2S_2O_8]$ = 33.3 g/l, $[Na_2S_2O_3.5H_2O]$ = 6.7 g/l, leaching time = 7 min, and T = 20°C.

Influence of $Na_2S_2O_3.5H_2O$ concentration

Figure 3-16 shows the effect $Na_2S_2O_3.5H_2O$ on the leaching behaviour of nickel. A plateau at the very beginning of the $Na_2S_2O_3.5H_2O$ addition (optimum at concentration of 0.1g/l) is observed where the total leaching efficiency reached (96 ± 0.6)%. The results in the figure agree with the literature [45] [46] which found that low concentration of thiosulfate is required for the leaching to start. As explained in section 3 $Na_2S_2O_3.5H_2O$ is required to remove the passive film from the surface of nickel following reaction 2.1

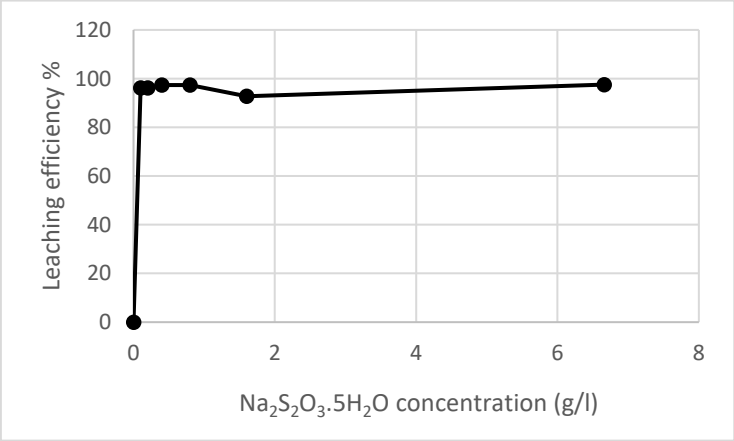

Figure 3-16 The effect of $Na_2S_2O_3.5H_2O$ concentration on the leaching efficiency. [NH_3] =5 M, $[(NH_4)_2S_2O_8]$ = 33.3 g/l, leaching time = 7 min, and T = 20°C.

Influence of $(NH_4)_2S_2O_8$ concentration

The presence of $(NH_4)_2S_2O_8$ is important since the $S_2O_8^{2-}$ acts as an oxidation agent in the leaching process and responsible to provide the system with N^{2+} following reaction 3.2 in section 3.1. [48] [49]

Varying the $(NH_4)_2S_2O_8$ concentration shows in **Figure 3-17** that 0 g/l concentration did not result in leaching when the NH_3 concentration is 5M. Moreover, the leaching efficiency at 6.7 g/l of $(NH_4)_2S_2O_8$ reached 92.7% at the same NH_3 concentration. The highest leaching efficiency was (98.1±0.6)% at $(NH_4)_2S_2O_8$ concentration of 30g/l where precipitates of

brownish chips were observed. The brownish chips are possibly released from the iron-rich part of the diffusion region and some nickel from the same region is co-released into the solution. The extra nickel that is co-released is responsible for the increase in the leaching efficiency. Nevertheless, the assumption that iron and extra nickel are released requires validation.

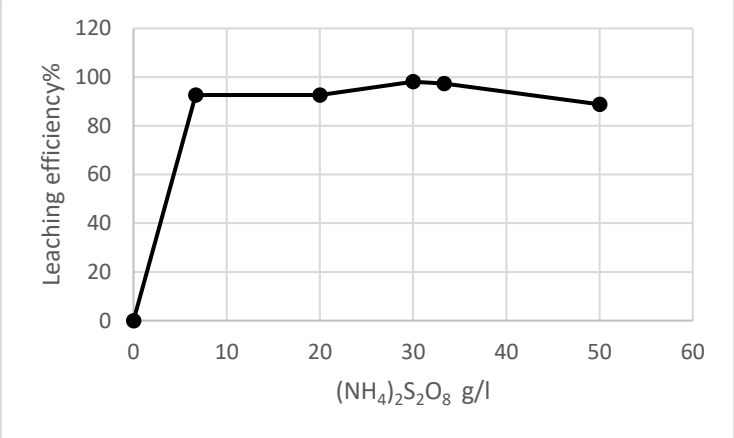

Figure 3-17 The effect of $(NH_4)_2S_2O_8$ concentration on the leaching efficiency. [NH_3] =5 M, [$Na_2S_2O_3.5H_2O$] = 0.1 g/l, leaching time = 7 min, and T = 20^oC.

Influence of Solid-to-Liquid (S/L) ratio

The S/L ratio is calculated considering the total mass of the sample divided by the volume of the ammoniacal solution in g/ml. The performed experiments to define the optimum solid to liquid ratio are different than these related to the rest of the report in terms of the solution volume and the number of samples submerged into the solution. The solution volume for each experiment was 240 ml. For the S/L = 1/37, 1/19, 1/10, and 1/6 the number of samples was 1, 2, 4, and 6 respectively. All the sample were of 2A type and the size of each was 50×50 mm^2.

The results of the S/L ratio experiments, presented in **Figure 3-18**, indicate minimal differences in leaching efficiencies. Observing the sample surfaces after leaching provided important information about the reason behind the difference.

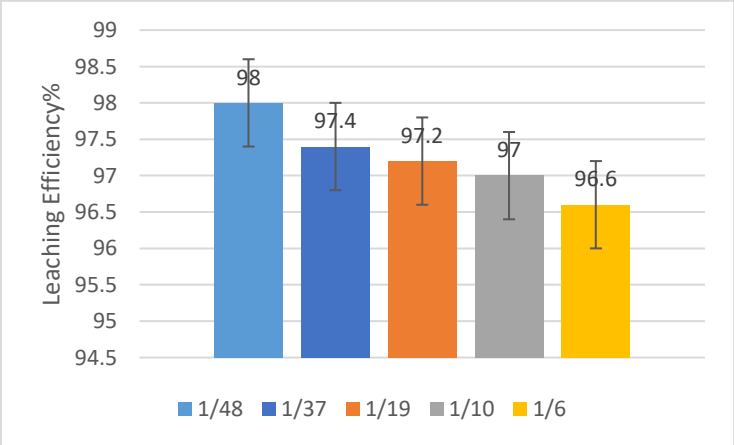

Figure 3-18 The effect of the solid liquid ratio on the total leaching efficiency. [$(NH_4)_2S_2O_8$] = 30g/l, [NH_3] =5 M, [$Na_2S_2O_3.5H_2O$] = 0.1 g/l, leaching time = 7 min, and T = 20^oC.

The samples with high solid-to-liquid (S/L) ratio exhibit partially leached areas, as shown in **Figure 3-19**. This occurs because the samples are positioned too closely, limiting the space for the solution to flow effectively between them.

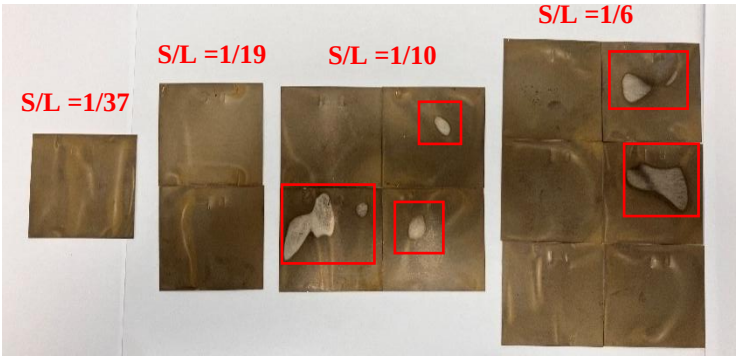

Figure 3-19 The leached samples that were used to determine the optimum S/L ratio. The red squares mark the regions where the nickel coating was not removed homogeneously as the rest of the samples' surfaces.

The S/L ratio provides a good estimation for the volume of solution required for industrial upscaling. However, the surface area to liquid ratio should also be considered. This is due to the nature of the reaction occurring on the surface of nickel. The larger the surface area exposed to leaching, the faster the dissolution of nickel.

3.6 System NH_3-$(NH_4)_2SO_4$- $Na_2S_2O_3.5H_2O$ -H_2O_2

Kinetics

Investigating the kinetics of the leaching process and reaching the optimum process parameters is essential for the upscaling the process to an industrial level. Parameters like leaching time, temperature, chemicals concentrations, and S/L ratio are important to reach the highest leaching efficiency.

Influence of time

The influence of leaching time on the leaching efficiency was investigated and the results are shown in **Figure 3-20.** The highest leaching efficiency (89.8 ± 0.6)% was observed at 2 minutes of leaching. The leaching efficiency at early stages of leaching, 30 seconds and 1 minute, was below 50%. While at 2 minutes and longer leaching efficiency did not significantly change. Therefore, 2 minutes was taken as the optimum leaching time.

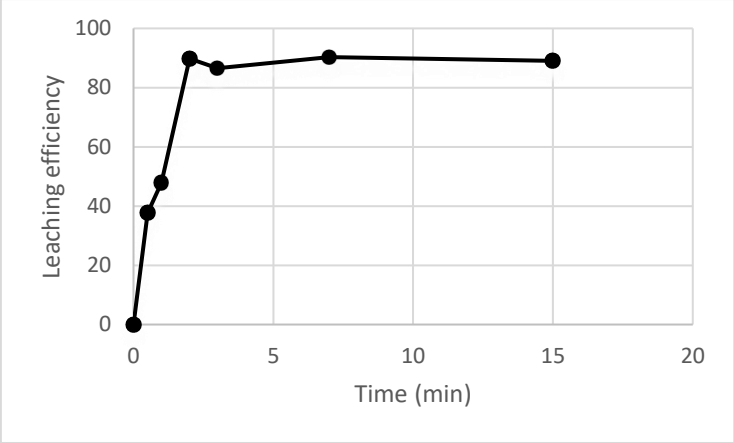

Figure 3-20 Influence of time on leaching efficiency with $[NH_3]$ = 2 M, $[(NH4)_2SO_4]$ = 40 g/l, $[Na_2S_2O_3.5H_2O]$ = 6.7 g/l, T = 40°C, aeration time = 30 min at rate of 5 l/min, and H_2O_2 35% = 16.7 ml/l

Influence of temperature

It can be seen from **Figure 3-21** that increasing temperature from room temperature to 40°C slightly increased the leaching efficiency. The highest leaching efficiency (94 ± 0.6) %was obtained at 80°C. It was noticed that the solution started to boil at 50°C and boiling became aggressive at 80°C and the solution escaped the beaker. Therefore, the optimum temperature was chosen to be 40°C since the difference in leaching efficiency is less than 2% and the solution remains stable inside the beaker.

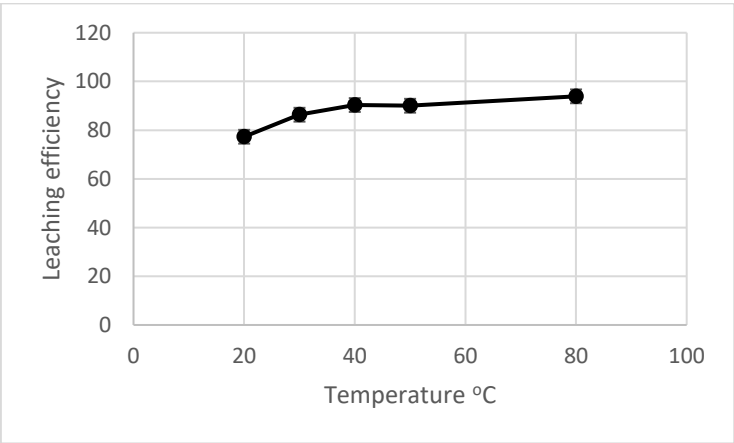

Figure 3-21 Influence of temperature on leaching efficiency with $[NH_3]$ = 2 M, $[(NH_4)_2SO_4]$ = 40 g/l, $[Na_2S_2O_3.5H_2O]$ = 6.7 g/l, t = 2 min, aeration time = 30 min at rate of 5 l/min, and H_2O_2 35% = 16.7 ml/l

Influence of aeration time

The purpose of aeration is to provide the solution with the required oxygen to oxidise the nickel prior to the formation of nickel hexamine in the ammoniacal solution. The lab results showed that the duration of aeration has almost no influence on the leaching efficiency in the presence of H_2O_2 in the solution. **Figure 3-22** shows the leaching efficiencies of 7 samples, each of them is leached under different aeration scenario as indicated in **Table 3-1**. The efficiency at long aeration times might slightly decrease due to the evaporation of ammonia.

Leaching efficiency under no aeration condition is high enough to eliminate the aeration parameter from the process to save time and to avoid the complexation of the experimental setup. The reason behind the slight influence of aeration is that the oxygen in the system is provided by a stronger oxygenator and that is H_2O_2.

Table 3-1 Aeration condition and duration per experiments

Sample number	Aeration scenario at rate of 5 l/min
1	no aeration during experiment
2	Aeration only during the experiment
3	5
4	10
5	20
6	30
7	60

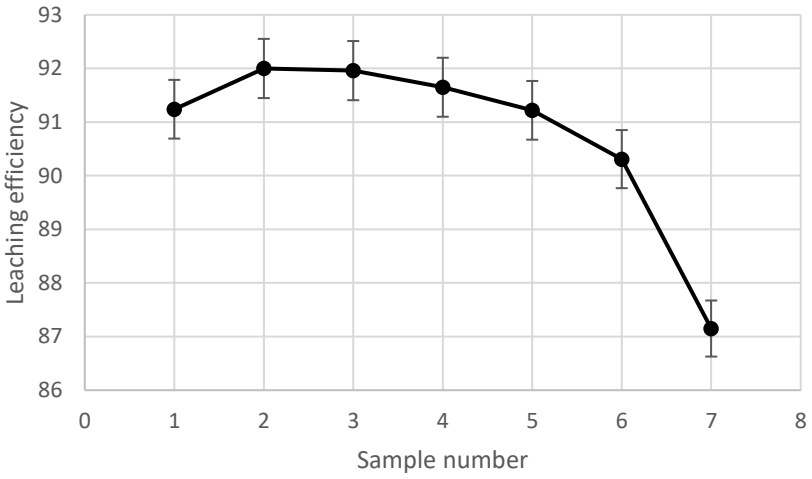

Figure 3-22 Influence of aeration scenario on the leaching efficiency with $[NH_3]$ = 2 M, $[(NH_4)_2SO_4]$ = 40 g/l, $[Na_2S_2O_3.5H_2O]$ = 6.7 g/l, t = 2 min, T =40^oC, and H_2O_2 35% = 16.7 ml/l. Note that the solutions for samples 3,4,5,6, and 7 were also aerated during the experiment.

With the absence of H_2O_2, the influence of leaching time on leaching efficiency was investigated again and it is found that the process requires longer leaching times compared with the solution containing H_2O_2. It can be seen from **Figure 3-23** that at 150 minutes of leaching, the total leaching efficiency remained as low as 26%. The longer leaching time and the lower leaching efficiency are not favourable in industrial scale implementation.

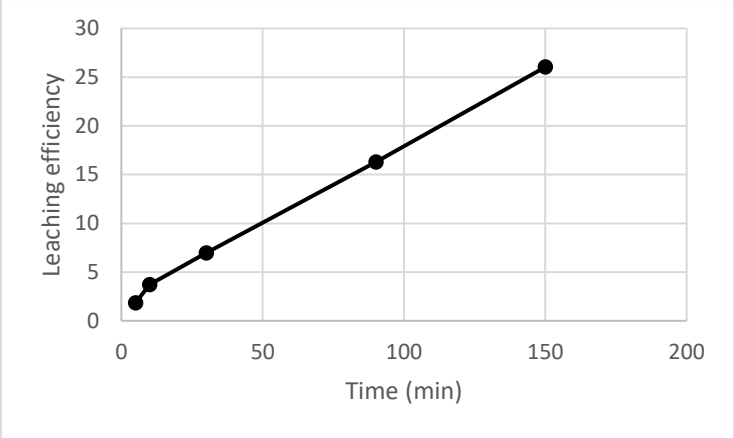

Figure 3-23 influence of time on leaching efficiency with [NH_3] = 2 M, [$(NH_4)_2SO_4$] = 40 g/l, [$Na_2S_2O_3.5H_2O$] = 6.7 g/l, aeration time = 30 min at rate of 5 l/min, aeration remained running during the experiment.

Influence of H_2O_2 concentration

Hydrogen peroxide H_2O_2 is highly effective in providing the required oxygen to the ammoniacal solution. As experimentally observed, with results shown in **Figure 3-24**, that the optimum leaching efficiency can be obtained at H_2O_2 concentration of 10 ml/l where the leaching efficiency at this concentration is about (93 ± 0.6)%. Lower H_2O_2 concentration yields lower leaching efficiency and higher concentrations does not further enhance the leaching efficiency. The role of oxygen is similar to that for $S_2O_8^-$. It is required to react, according to reaction (3.4) with the metallic Ni to produce Ni^{2+} which in turn reacts with NH_3 to produce $Ni(NH_3)_6^{2+}$ following reaction (3.3)

$$Ni + H_2O_2 \rightarrow Ni^{2+} + 2OH^- \quad (3.4)$$

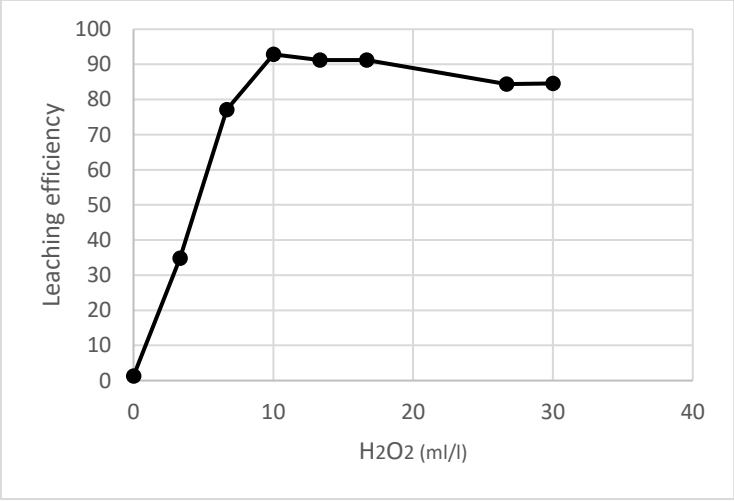

Figure 3-24 influence of H_2O_2 on the leaching efficiency [NH_3] = 2 M, [$(NH_4)_2SO_4$] = 40 g/l, [$Na_2S_2O_3.5H_2O$] = 6.7 g/l, T = 40^oC.

Influence NH_3 concentration.

The leaching experiments to find the optimum ammonia concentration, in **Figure 3-25** show that leaching of nickel is possible even without adding NH_3 to the solution. Preparing a solution consisting of distilled water, $(NH_4)_2SO_4$, $Na_2S_2O_3.5H_2O$, and H_2O_2, will be sufficient to start the leaching process. That is possibly due to the dissociation of $(NH_4)_2SO_4$ in water that produces NH_3. However, to reach higher leaching efficiencies, it is required to add NH_3.

The leaching efficiency at $[NH_3]$ of 1.5 M reached (93 ± 0.6)%. The efficiency at higher concentrations did not change considerably. The leaching curve starts to show a plateau like behaviour at concentration of 1.5 M. therefore, the optimum NH_3 concentration is 1.5 M.

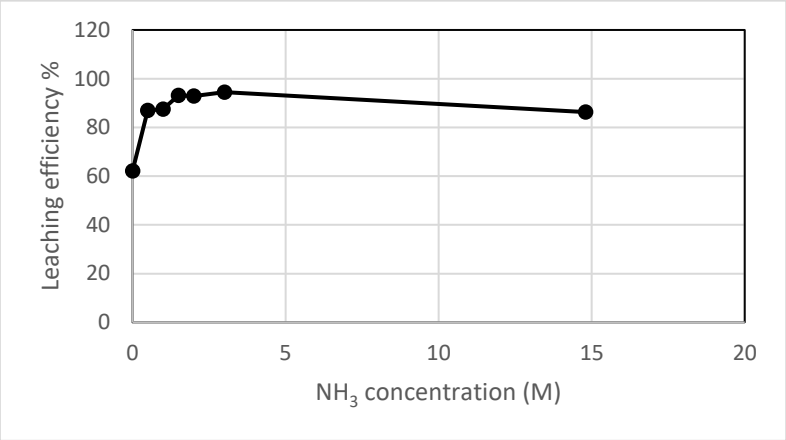

Figure 3-25 the effect of NH_3 concentrations on the leaching efficiency. $[(NH_4)_2SO_4]$ = 40 g/l, g/l, T = 40°C, $[Na_2S_2O_3.5H_2O]$ = 6.7 g/l, time = 2 min, and H_2O_2 35% solution = 10 ml/l.

Influence of $Na_2S_2O_3.5H_2O$ concentration

The performed experiments on the effect of $Na_2S_2O_3.5H_2O$ concentration, see results in **Figure 3-26**, showed that the absence of $Na_2S_2O_3.5H_2O$ yielded leaching with efficiency equals to zero. In addition, a small amount of $Na_2S_2O_3.5H_2O$ was required to reach relatively high leaching efficiency. The optimum $Na_2S_2O_3.5H_2O$ was found to be 0.42 g/l and yielded a total leaching efficiency of (91±0.6)%. The efficiency at 0.025 g/l was (54.5 ± 0.6%) indicating that $Na_2S_2O_3.5H_2O$ was consumed to remove parts of the passive film. That was supported by the presence of intact regions on the surface of the sample.

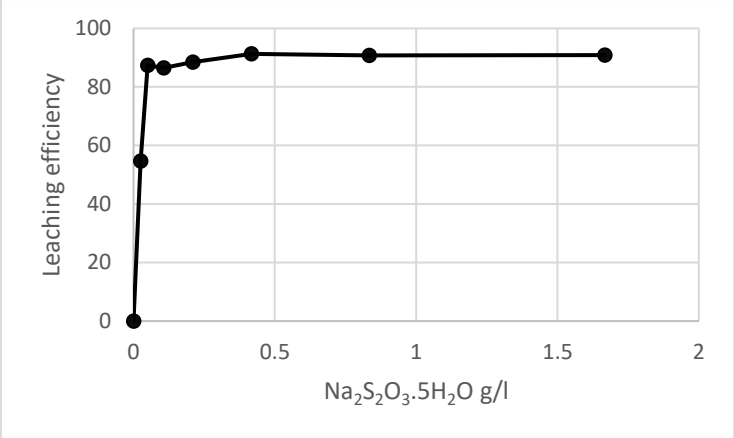

Figure 3-26 Effect of $Na_2S_2O_3.5H_2O$ concentration on the leaching efficiency. $[(NH_4)_2SO_4]$ = 40 g/l, $[NH_3]$ =1.5 M, T = 40°C, time = 2 min, and H_2O_2 35% solution = 10 ml/l.

Influence of $(NH_4)_2SO_4$ concentration

The rule of $(NH_4)_2SO_4$ is influential to the leaching process as can be noticed from **Figure 3-27**. The absence of $(NH_4)_2SO_4$ prohibit the leaching process. A study into the potential of the dissolution of nickel in the absence and the presence of $(NH_4)_2SO_4$ is required to clarify the reason behind this behaviour. On the other hand, adding 6.7 g/l of $(NH_4)_2SO_4$ allowed leaching to start and higher concentrations were required for higher efficiencies. The leaching efficiency at 40 g/l was as high as 91.3% where the leaching curve starts to show a plateau behaviour in the figure. Therefore, the 40g/l is taken as the optimum concentration of $(NH_4)_2SO_4$.

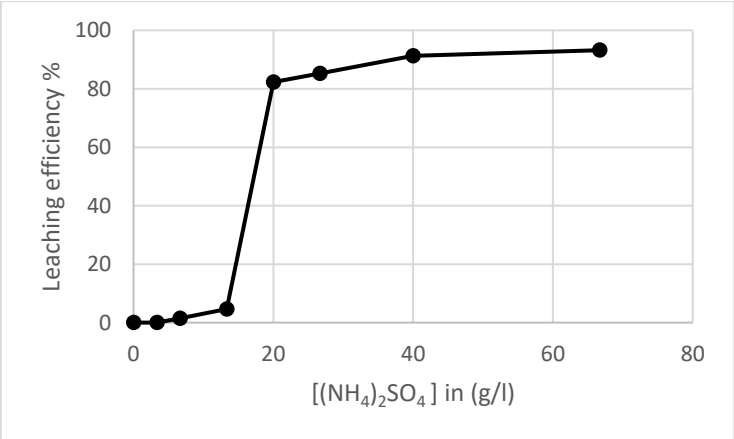

Figure 3-27 Effect of $(NH_4)_2SO_4$ concentration on the leaching efficiency. [NH3] =1.5 M, T = 40°C, $[Na_2S_2O_3.5H_2O]$ = 0.40 g/l, time = 2 min, and H_2O_2 35% solution = 10 ml/l.

3.7 Nickel removal from end-of-life Li-ion battery casings

Two end-of-use Li-ion batteries from the same source and type were dissembled, and their casings were subjected to leaching in two different solutions. The first sample, labelled as LB1 in **Figure 3-28**, was immersed in the solution with the optimum parameters obtained for the system NH_3-$Na_2S_2O_3.5H_2O$-$(NH_4)_2S_2O_8$. The second sample, labelled as LB2, was subjected to leaching in the optimised system NH_3-$Na_2S_2O_3.5H_2O$-$(NH_4)_2SO_4$-H_2O_2. The measured nickel content on both samples before leaching was 21 g/m^2.

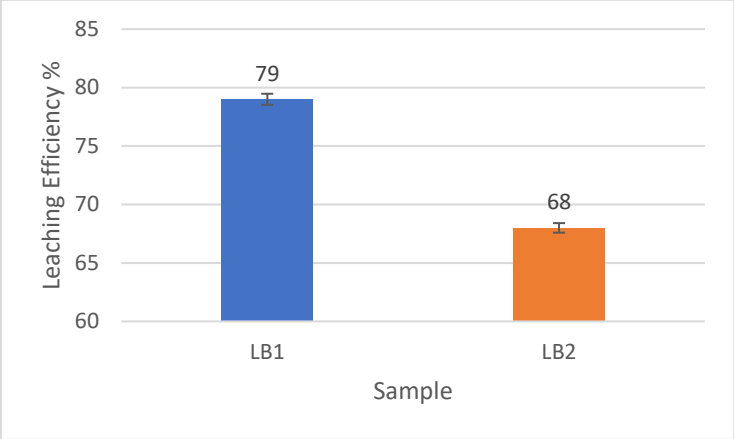

Figure 3-28 the leaching efficiencies for Li-ion battery casings. LB1 is leached with the optimised NH_3-$(NH_4)_2S_2O_8$- $Na_2S_2O_3.5H_2O$. System, and LB2 is leached with the optimised NH_3-$(NH_4)_2SO_4$- $Na_2S_2O_3.5H_2O$ -H_2O_2 system.

The efficiency for sample LB1 was 79% and for LB2 68%. The results here are lower than the results for the 2A samples. The most applaudable reason is that the diffusion region between the nickel coating and the steel substrate is larger than it for the 2A samples due to longer annealing time after coating.

3.8 Leaching of zinc, copper, and cobalt

The leaching experiments to investigate the dissolution of zinc, copper, and cobalt were carried out in the system NH_3-$(NH_4)_2S_2O_8$- $Na_2S_2O_3.5H_2O$. The only purpose of these experiment is showing the capability of the NH_3-$(NH_4)_2S_2O_8$- $Na_2S_2O_3.5H_2O$ system to dissolve three of the metals.

The leaching results for copper and cobalt are shown in **Figure 3-29**. The initial weights of the copper and the cobalt samples were 21.6g and 5.5g respectively. The size of the copper sample was 50×50 mm^2 and the cobalt sample was of irregular shape and smaller than the

copper one as can be seen in **Figure 3-31**. The leaching efficiency for copper was 3.2% after 10 minutes of leaching while it was 2.5% after the same leaching time.

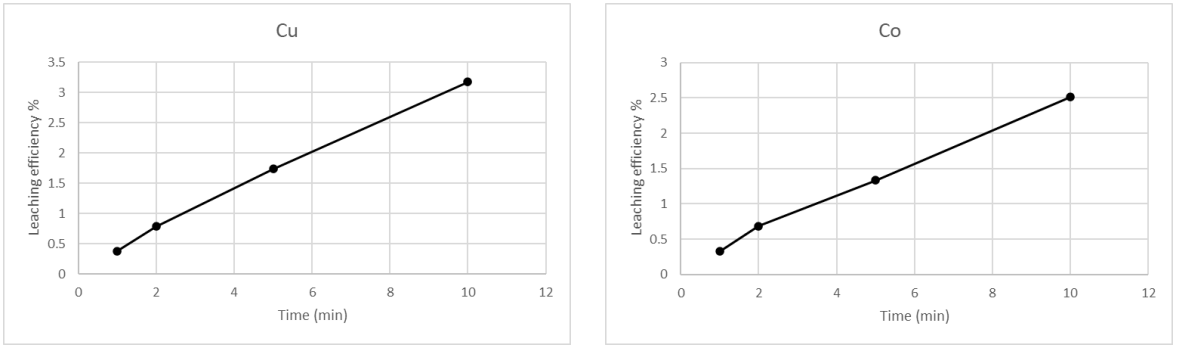

Figure 3-29 The weight loss of the copper on left and cobalt on right. The samples were leached in solutions of 300 ml volume with $[(NH_4)_2S_2O_8]$ = 30 g/l, $[NH_3]$ =5 M, $[Na_2S_2O_3.5H_2O]$ = 0.4 g/l, T= 20°C.

The zinc coating with content of 83 ± 2.7 g/m^2 on the zinc-plated steel (ZPS) specimen was totally removed and dissolved in the ammoniacal solution leading to leaching efficiency of 100% as can be seen from **Figure 3-30**.

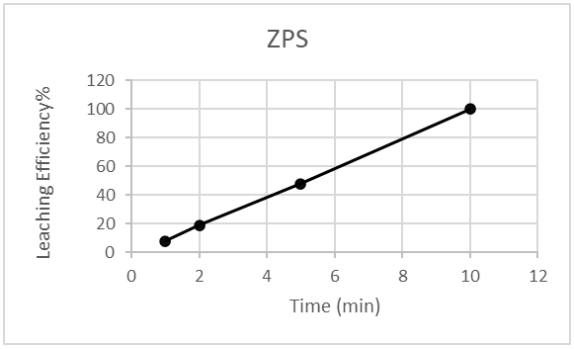

Figure 3-30 The leaching efficiency of the zinc coated steel sample leached in solutions with $[(NH_4)_2S_2O_8]$ = 30 g/l, $[NH_3]$ =5 M, $[Na_2S_2O_3.5H_2O]$ = 0.4 g/l, T= 20°C. The experiment was performed in a 300 ml beaker.

Since the used samples are different in weight, size, and purity, nothing can be concluded regarding which of the three has the highest leaching efficiency. On the other hand, it can be well concluded that the ammoniacal solution can selectively leach each of the three metals if plated on steel.

Figure 3-31 shows that the dissolution of cobalt, copper, and nickel in the ammoniacal solutions is contributed to the formation of orange, dark blue, and blue colours respectively. Moreover, the dissolution of zinc in ammonia does not change the solutions colour.

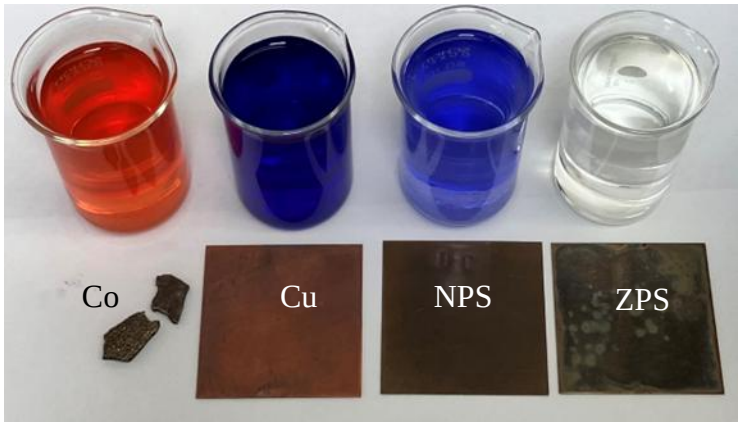

Figure 3-31 Co, Cu, NPS, and ZPS samples and their leaching solutions after performing the leaching experiment.

It was observed experimentally that the dissolution of Co is similar to Ni. It is not possible without the addition of $Na_2S_2O_3.5H_2O$ to the solution in order to remove the cobalt oxide layer from the surface following reaction (3.5). In addition, the same experimental order for nickel dissolution should be followed to dissolve Co. After the removal of the oxide layer, the leaching process continues with oxidising the metallic cobalt to produce cobalt ions following reaction (3.6). Thereafter, the reaction between cobalt ions and the ammonia to form cobalt hexamine takes place following reaction (3.7).

$$Co + S_2O_3^{2-} \rightarrow CoS + SO_4^{2-} \quad 3.5$$

$$Co + S_2O_8^{2-} \rightarrow Co^{2+} + 2SO_4^{2-} \quad 3.6$$

$$Co^{2+} + 6NH_3 \rightarrow Co(NH_3)_6^{2+} \quad 3.7$$

The dissolution of copper in the ammoniacal solution does not require the addition of $Na_2S_2O_3.5H_2O$. The reaction starts with oxidising the copper following in reaction 3.8 then the formation of copper amine as can be seen in reactions (3.8) and (3.9) respectively.

$$Cu + S_2O_8^{2-} \rightarrow Cu^{2+} + 2SO_4^{2} \quad 3.8$$

$$Cu^{2+} + 4NH_3 \rightarrow Cu(NH_3)_4^{2+} \quad 3.9$$

Similar to copper, zinc does not need the addition of $Na_2S_2O_3.5H_2O$ and requires oxidation prior to the formation of zinc amine following reactions (3.10 and 3.11)

$$Zn + S_2O_8^{2-} \rightarrow Zn^{2+} + 2SO_4^{2-} \quad 3.10$$

$$Zn^{2+} + 4NH_3 \rightarrow Zn(NH_3)_4^{2+} \quad 3.11$$

4 Process feasibility on industrial scale.

In this section a cost indication for the leaching process for industrial scale will be carried out alongside a discussion around the minimum requirement of the industrial leaching installation.

4.1 Cost Indication

The cost of the materials involved in the leaching process is analysed based on the market prices that are published online. In addition, the optimum conditions of the system NH_3-$Na_2S_2O_3.5H_2O$ -$(NH_4)_2S_2O_8$ will be considered in the analysis. The input and output materials of the process are listed in **Table 4-1**, with their prices and the total cost of the process considering that the proposed installation in **Figure 4-1** has a capacity of 1 m^3 of the ammonium solution with NH_3 concentration of 5M. It is important to consider that ammonia is recoverable and can be reused. Moreover, the cost indication considers a S/L ratio of 1/6 with NPS of type 2A and thickness of 0,3 mm.

Table 4-1 Cost indication for the leaching process.

Input Material	Price	Required amount /m^3 of solution	Input Total cost €
NH_3 in water 25%*	570 €/m^3 [50]	338 L	193
$(NH_4)_2S_2O_8$	1 €/Kg [51]	30 Kg	30
$Na_2S_2O_3.5H_2O$	1.8 €/Kg [50]	0.4 Kg	0.7
Water	4 €/m^3 [52]	662 L	2.6
NPS (2A)	0.1 €/Kg [53]	167 Kg	16.7
		Total cost of input materials	243
Output material	Price	Produced amount/ m^3 of solution	Output Total cost €
Nickel	17 €/Kg [54]	3.2 Kg	54.4
NH_3 in water 25%*	570 €/m^3	304.2 L	173
Clean Steel scrap	0.17 €/ Kg [53]	163.8 Kg	27.8
		Total price of output materials	255.2
		Net cost (Input + output)	255.2- 243 = 12.2 €
*Assuming that NH_3 is 90% recoverable.			

What the table shows is that the removal process will provide a value of 12.2 € from each m^3 of the leaching solution at S/L ratio of 1/6. The price indication assumes 10% of NH_3 consumption assuming that 90% of the NH_3 is recoverable . The value (12.2 €) should consider the cost of nickel recovery from the solution, the installation cost, labour, material transport, and other running costs. This is only under the optimum parameters that were obtained here in section 3.5 and this might change depending on further optimisations.

4.2 The industrial installation

Any industrial installation designed for the leaching process on an industrial scale must meet the necessary operational requirements. The primary consideration is ensuring the scrap surfaces are effectively exposed to the ammoniacal solution. This can be achieved by rotating the scrap within the solution while keeping the scrap cage fully and always submerged. The rotational motion of the scrap should prevent the scrap pieces from adhering to each other and allows the solution to flow in sufficient amount between the scrap pieces. Moreover, the addition of the required chemicals to the solution should follow the order that was experimentally specified. That is by dividing the process into three steps. The first step is the addition of water, ammonia, $Na_2S_2O_3.5H_2O$, and $(NH_4)_2SO_4$ if applicable. The second step is the addition of the scrap. The last step is the addition of $(NH_4)_2S_2O_8$ or H_2O_2.

The schematic drawing for the industrial installation in **Figure 4-1** shows a rotating scrap cage which will assure that the scrap surfaces will be efficiently subjected to the solution and therefore achieve the highest possible leaching efficiency. In addition, the installation has a separate feeding part for each input material to control the order of materials and scrap addition as required. The installation is equipped with a stirrer to allow the salts to dissolve into the solution and to enhance the kinetics of the reaction. A gas collector is also required to mainly collect the evaporated ammonia for reusing purposes. The installation is equipped with a heating source in case heating of the solution is required.

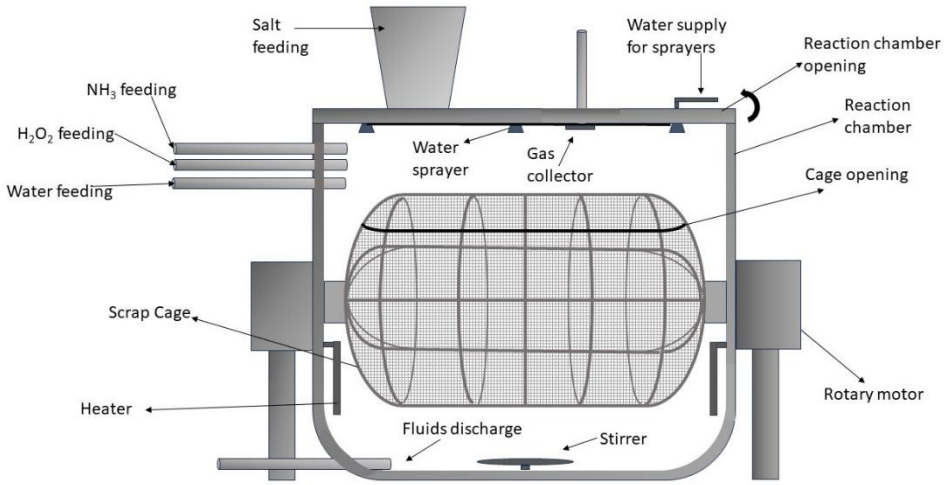

Figure 4-1 the suggested industrial installation for industrial scale leaching.

5 Conclusion, limitations, and recommendations

5.1 Conclusion

The experimental work related to the removal of nickel coating from the NPS factory offcuts has led to the development of two alternative ammoniacal systems. The first system is the NH_3-$Na_2S_2O_3.5H_2O$-$(NH_4)_2S_2O_8$ system where the $(NH_4)_2S_2O_8$ is used as an oxidant. The second system is the NH_3-$Na_2S_2O_3.5H_2O$-$(NH_4)_2SO_4$-H_2O_2 where the oxygen from H_2O_2 acts as an oxidant. The role of $Na_2S_2O_3.5H_2O$ in both systems is crucial to break the passive film on the nickel surface directly after immersing the sample in the solution.

The optimum leaching efficiency was (96.6 ± 0.6)% for the system NH_3-$Na_2S_2O_3.5H_2O$-$(NH_4)_2S_2O_8$ at leaching time = 7 minutes, leaching temperature = 20^oC, $[NH_3]$ = 5M, $[Na_2S_2O_3.5H_2O]$ = 0.1 g/l, $[(NH_4)_2S_2O_8]$ = 30 g/l, and S/L ratio of 1/6. For the system NH_3-$Na_2S_2O_3.5H_2O$-$(NH_4)_2SO_4$- H_2O_2, the optimum leaching efficiency was (91± 0.6)% at leaching time = 2 minutes, leaching temperature =40^oC, [NH3] = 1.5M, $[Na_2S_2O_3.5H_2O]$ = 0.4 g/l, $[(NH_4)_2SO_4]$ = 40 g/l, H_2O_2 35% solution = 10 ml/l. Higher leaching efficiencies for both system are difficult to obtain due to the formation of a passive film in the diffusion region between the nickel coating and the steel substrate. Therefore, it is important to consider minimising the diffusion region during the annealing of the NPS sheet.

The nickel coatings from the end-of-use Li-ion battery casings were partially removed with leaching efficiencies of 79% for the system that contain $(NH_4)_2S_2O_8$ and 68% for the system where oxygen is used as an oxidant. The lower leaching efficiency is probably related to the wider diffusion region between the nickel coating and the steel substrate.

Copper, zinc, and cobalt can also be dissolved into the same ammoniacal solutions as used for nickel removal. In the case of cobalt, it follows the same procedure as for nickel, i.e. the sample should be immersed into the solution before the oxidant. While for copper and zinc, the sample can be added after the addition of the oxidant into the solution.

The work done on nickel, cobalt, copper, and zinc leaching lead to the filling of two patent applications. The first one is related to the leaching of nickel and cobalt following the same method developed in sections 3.1 and 3.2 with keeping the same experimental order. The second patent is related to zinc and copper leaching while keeping the experimental order and the need for $Na_2S_2O_3.5H_2O$ is not required.

5.2 Limitations

- This study does not experimentally cover the methods that are capable to recover the nickel from the ammoniacal solution after dissolution. The solutions after leaching does not only have nickel amine complexes but also sulphate compounds. Therefore, selective recovery of nickel is needed.

5.3 Recommendations

- Employ a UV-VIS (Ultraviolet-Visible) spectroscopy investigations to find the rate of the reactions, and the produced compounds during the leaching process for better understanding of the thermodynamics and the kinetics of the system.
- Constructing a new parameter for the leaching process and that is the Surface-Area-to-Liquid ratio. The surface area is an important parameter in the leaching of coated materials. Tow samples with the same mass and with two different surface areas will

need different leaching times and the one with higher surface area will dissolve in shorter time.

6 Appendix A

SEM, EDX, and XPS analysis for the NPS samples, type 2A, before and during leaching.

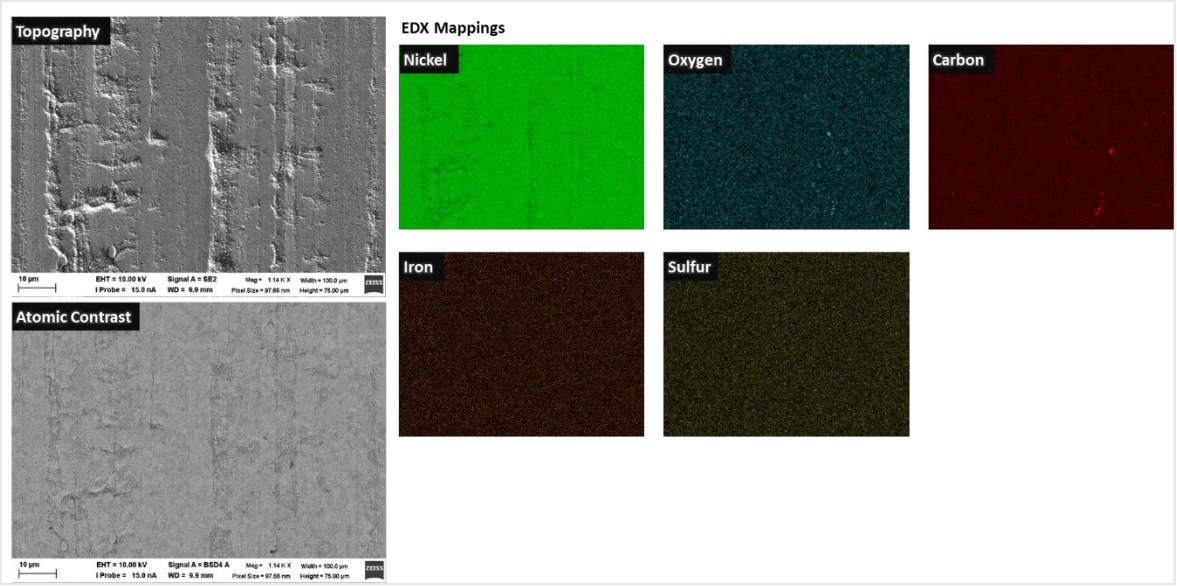

Figure 6-1 Elemental mapping for the surface of side 2 of the reference sample.

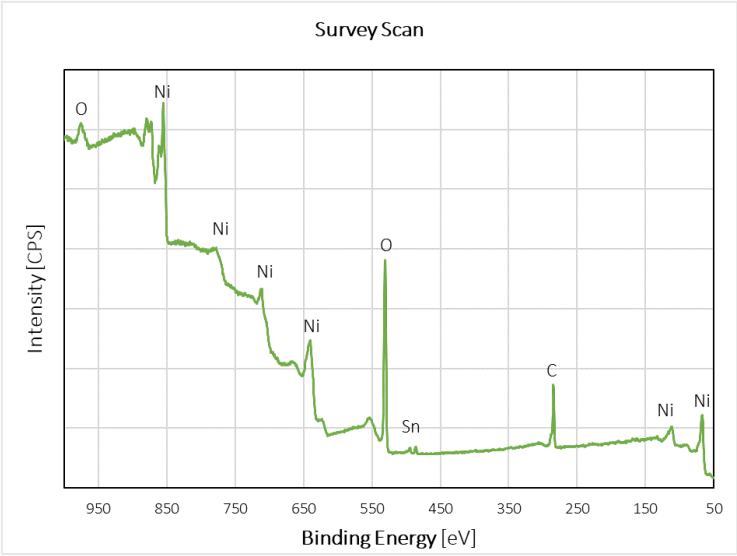

Figure 6-2 XPS scan for the surface of side 2 of the reference sample.

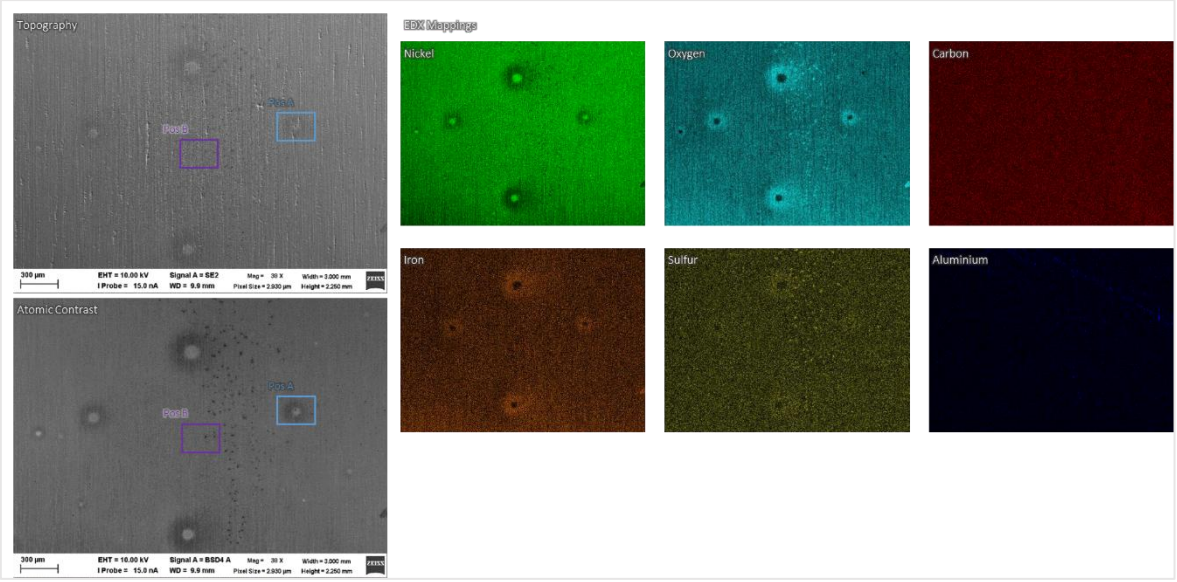

Figure 6-3 Elemental mapping for the surface of side 2 after 20 seconds of leaching in the NH_3-$(NH_4)_2SO_4$-$Na_2S_2O_3.5H_2O$-H_2O_2 System.

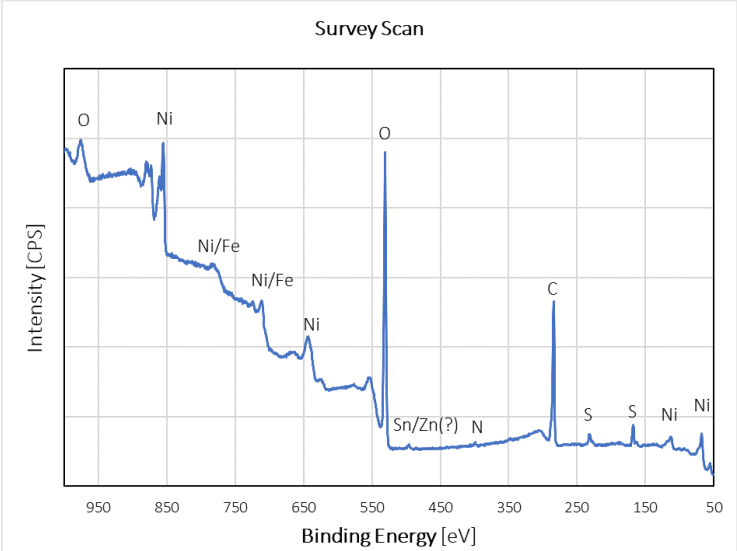

Figure 6-4 XPS scan for the surface of side 2 after 20 seconds of leaching in the NH_3-$(NH_4)_2SO_4$-$Na_2S_2O_3.5H_2O$-H_2O_2 System

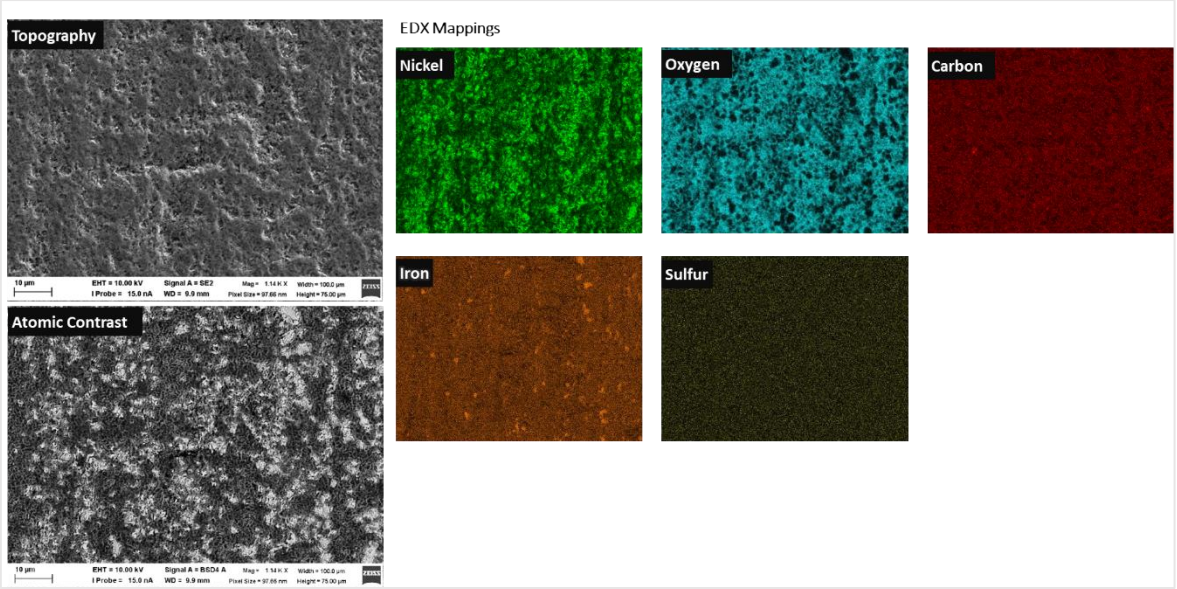

Figure 6-5 Elemental mapping for side 2 after 420 seconds of leaching in the NH_3-$(NH_4)_2SO_4$-$Na_2S_2O_3.5H_2O$-H_2O_2 System.

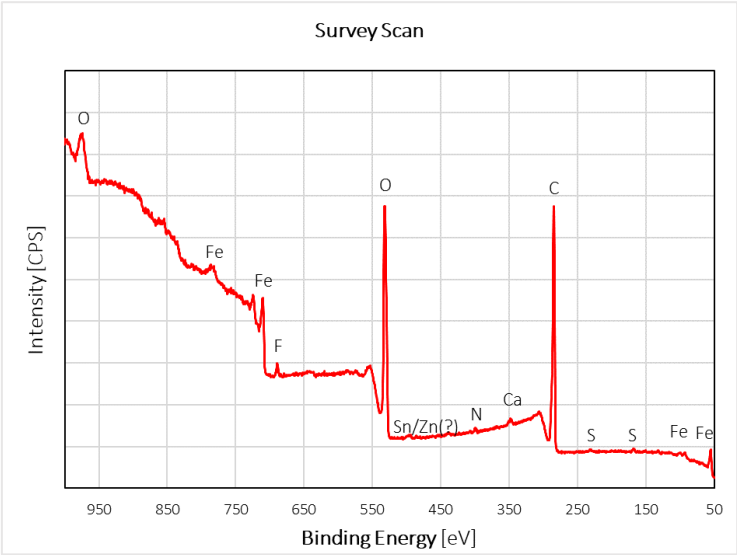

Figure 6-6 XPS scan for the side 2 after 420 seconds of leaching in the NH_3-$(NH_4)_2SO_4$-$Na_2S_2O_3.5H_2O$-H_2O_2 System.

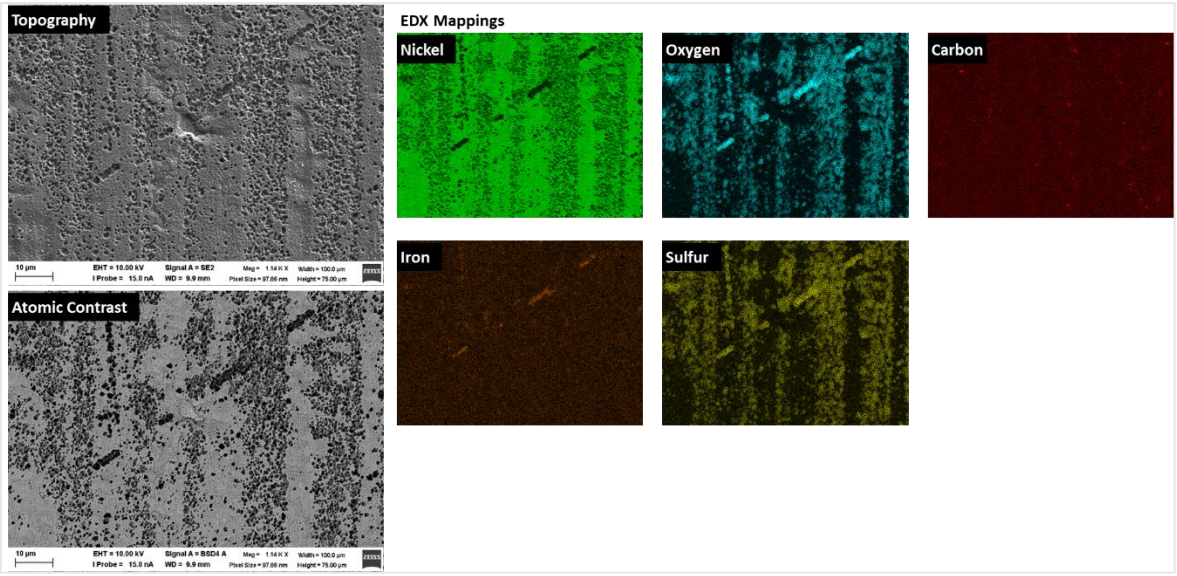

Figure 6-7 Elemental mapping of side 2 after 20 seconds of leaching in the NH_3-$(NH_4)_2S_2O_8$-$Na_2S_2O_3.5H_2O$ system.

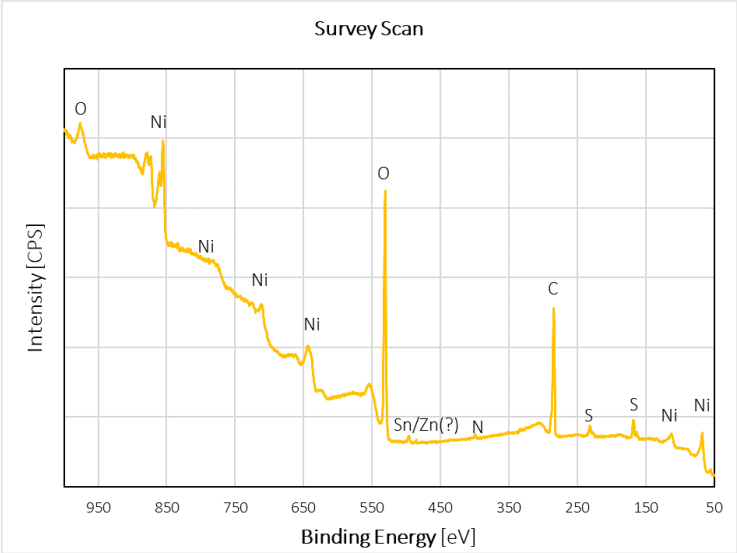

Figure 6-8 XPS scan for side 2 after 20 seconds of leaching in the NH_3-$(NH_4)_2S_2O_8$-$Na_2S_2O_3.5H_2O$ system.

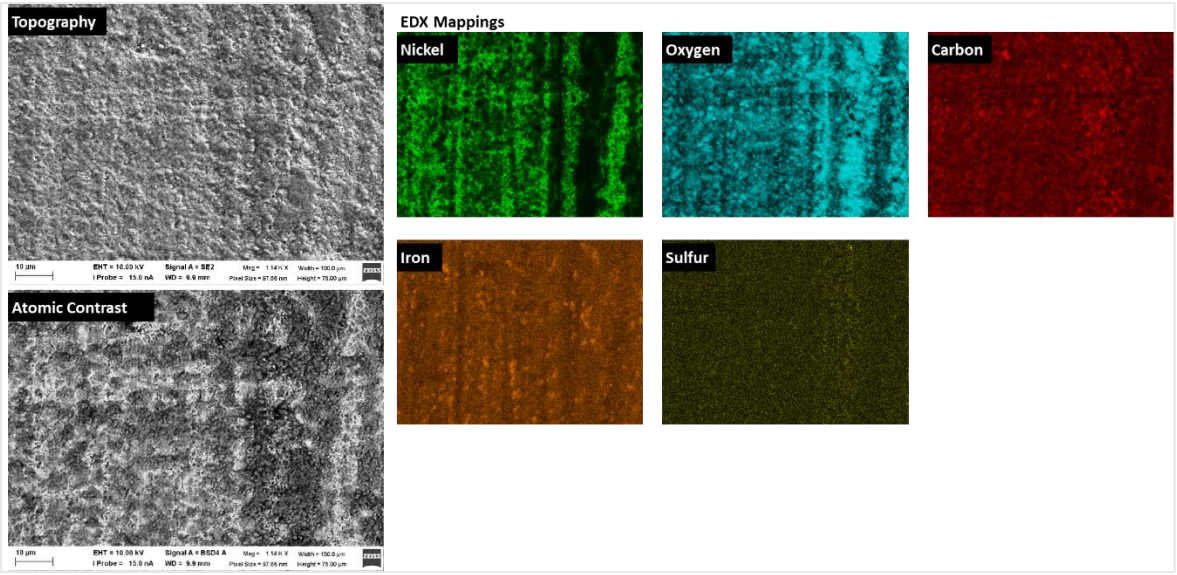

Figure 6-9 Elemental mapping for side 2 after 420 seconds of leaching in the NH_3-$(NH_4)_2S_2O_8$- $Na_2S_2O_3.5H_2O$ system.

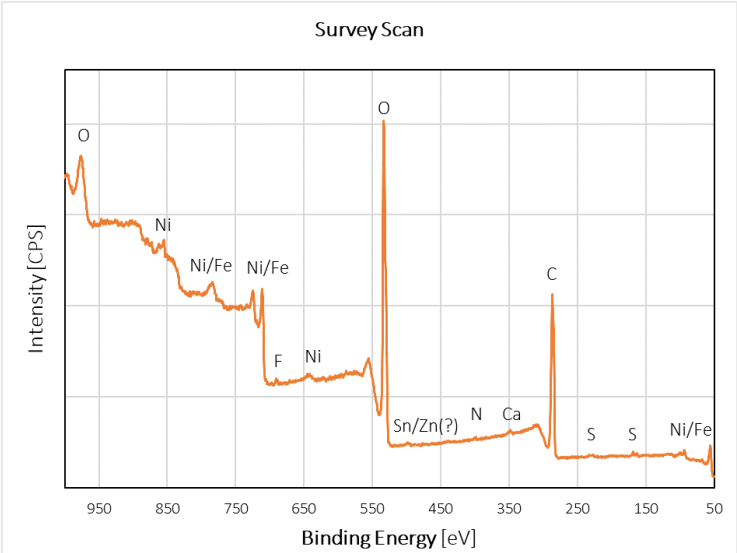

Figure 6-10 XPS scan for the surface of side 2 after 20 seconds of leaching in the NH_3-$(NH_4)_2S_2O_8$- $Na_2S_2O_3.5H_2O$ system.

7 Appendix B

GDOES results for NPS.

Side 1

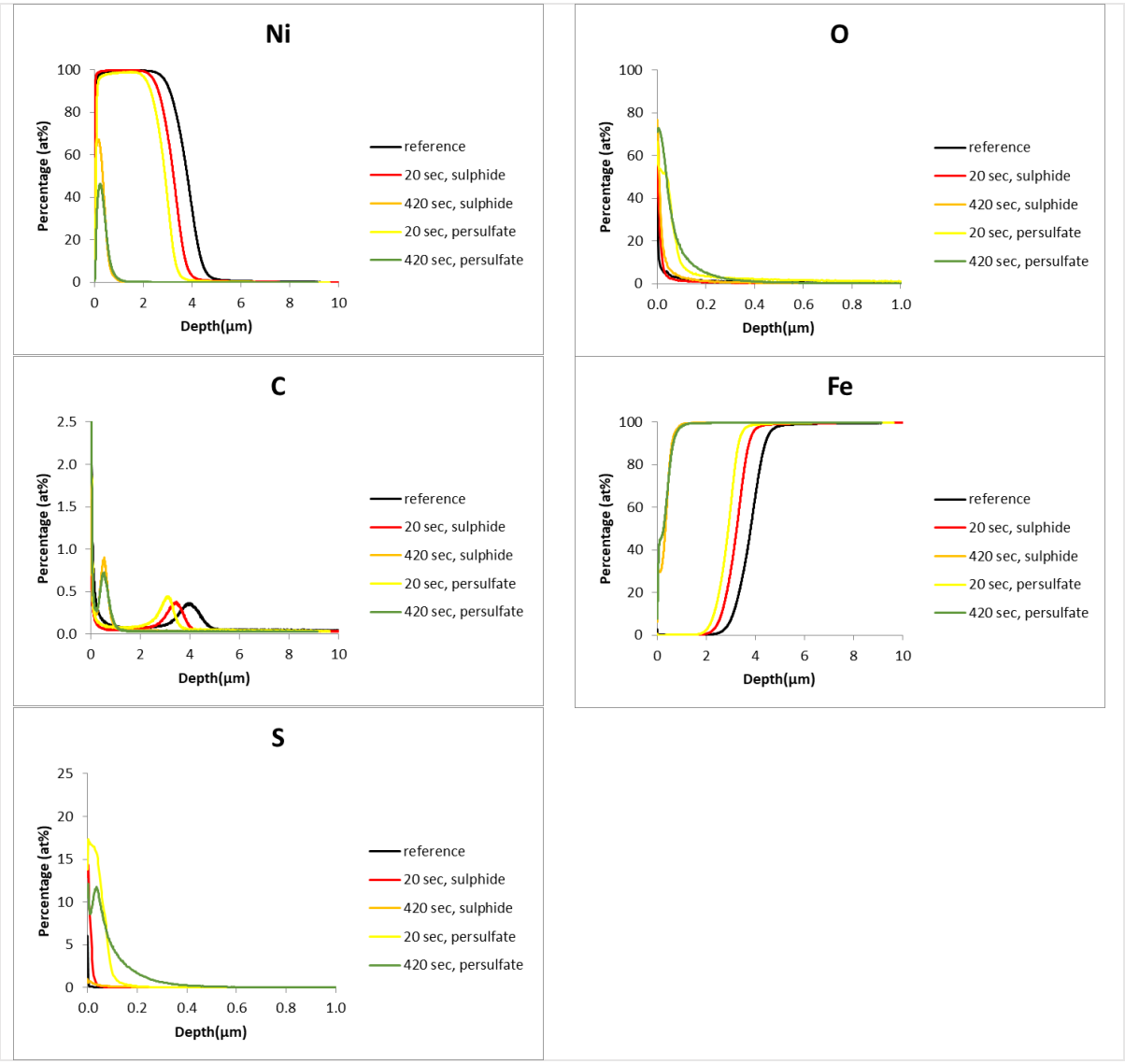

Figure 7-1 GDOES results taken from the surface of side 1 of the for the reference sample and the samples after 20 and 420 seconds of leaching in two different ammoniacal systems. NH_3-$(NH_4)_2S_2O_8$- $Na_2S_2O_3.5H_2O$, mentioned as persulfate in the figure. The other one is NH_3-$(NH_4)_2SO_4$-$Na_2S_2O_3.5H_2O$-H_2O_2, mentioned as sulphide in the figure.

Side 2

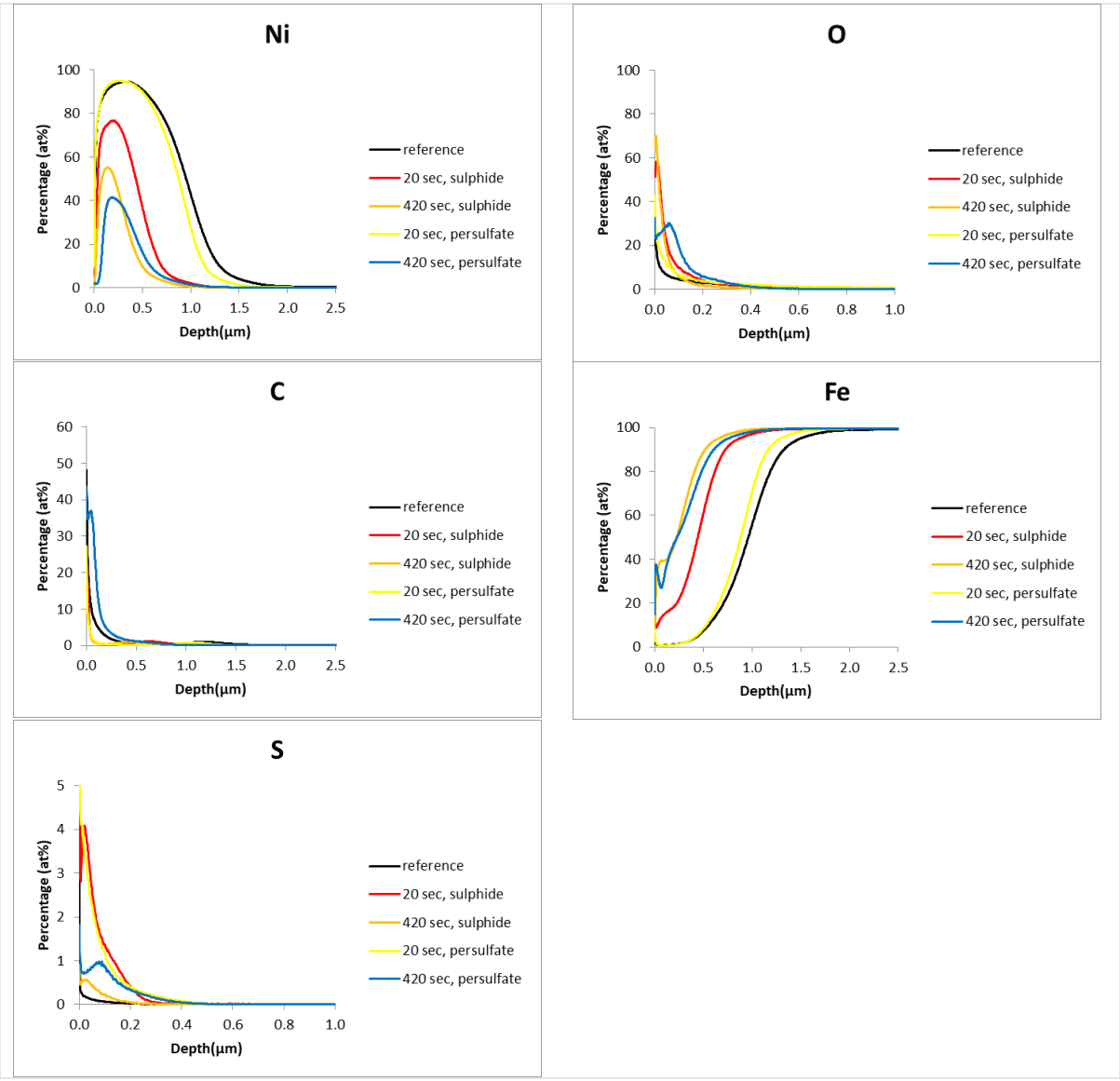

Figure 7-2 GDOES results taken from the surfaces of side 2 for the reference sample and the samples after 20 and 420 seconds of leaching in two different ammoniacal systems. NH_3-$(NH_4)_2S_2O_8$- $Na_2S_2O_3.5H_2O$, mentioned as persulfate in the figure, and NH_3-$(NH_4)_2SO_4$-$Na_2S_2O_3.5H_2O$-H_2O_2, mentioned as sulphide in the figure.

References

[1] *Nickel Plating Handbook,* Nickel Institute, 2014.

[2] N. Campagnol, K. Hoffman, A. Lala, O Ramsbottom, “The future of Nickel: A class act,” 2017.

[3] Jannick Saegert, Vovia Witni and Marie Nerreter, “Nickel for the energy transition: a developmental perspective,” GIZ, 2022.

[4] M. Grohol, C. Veeh, “Study on the critical raw materials for the EU,” European Commision, Brussels, 2023.

[5] “A new Circular Economy Action Plan,” 2020. [Online]. Available: https://eur-lex.europa.eu/resource.html?uri=cellar:9903b325-6388-11ea-b735-01aa75ed71a1.0017.02/DOC_1&format=PDF. [Accessed April 2024].

[6] “Nickel institute,” [Online]. Available: https://nickelinstitute.org/en/policy/nickel-life-cycle-management/nickel-recycling/. [Accessed April 2024].

[7] IEA, “www.iea.org,” 2021. [Online]. Available: https://www.iea.org/data-and-statistics/charts/ghg-emissions-intensity-for-class-1-nickel-by-resource-type-and-processing-route. [Accessed 2024].

[8] Sonter, L. J., Lloyd, T. J., Kearney, S. G., Di Marco, M., O'Bryan, C.J., Valenta, R. K., & Watson, J. E. M., “Conservation implications and opportunities of mining activities for terrestrial mammal habitat,” *Conservation Science and Practice,* vol. 4, no. 12, 2022.

[9] “Achilles,” [Online]. Available: https://www.achilles.com/uncategorised/green-energy-dangers-the-social-impact-of-battery-mining-for-nickel/. [Accessed 29 March 2024].

[10] Bismarck Kwaku Asare, M. B. K. Darkoh, “SOCIO-ECONOMIC AND ENVIRONMENTAL IMPACTS OF MINING IN BOTSWANA: A CASE STUDY OF THE SELEBI-PHIKWE COPPER-NICKEL MINE,” *EASSRR,* vol. XVII, no. no. 2, June 2001.

[11] E. Naryono., “Nickel Mine Exploitation In Indonesia, Between A Blessing And A Disaster Of Environmental Damage,” *Center for Open Science,* 2023.

[12] Murdifin, Imaduddin/Pelu, Muhammad Faisal AR et. al, “Environmental disclosure as corporate social responsibility : evidence from the biggest nickel mining in Indonesia,” *International Journal of Energy Economics and Policy,* vol. 9, pp. 115 - 122, 2019.

[13] Sabine Dworak, Helmut Rechberger, and Johann Fellner, “How will tramp elements affect future steel recycling in Europe – A dynamic material flow model for steel in the

EU-28 for the period 1910 to 2050," *Resources, Conservation & Recycling,* vol. 179, 2022.

[14] G. Kleindschmidt, H.W. Gudenau,, "ECSC RTD Progam, Removal of impurities from scrap in HTM without and under vacuum," European Comission, 1991-1995.

[15] R.R. Moskalyk, A.M. Alfantaz, "Nickel laterite processing and electrowinning practice," *Minerals Engineering,* vol. 15, p. 593–605, 2002.

[16] Hwa Young Lee, Sung Gyu Kim, Jong Kee Oh, "Electrochemical leaching of nickel from low-grade laterites," *Hydrometallurgy,* vol. 77, p. 263–268, 2005.

[17] X. Hu, B. Ma, F He, Y. Chen and C. Wang, "Ammonia leaching process for selective extraction of nickel and cobalt from polymetallic mixed hydroxide precipitate," *Journal of Environmental Chemical Engineering.,* vol. 10, no. 6, 2022.

[18] Bharat Padh, P.C. Rout, G.K. Mishra, K.R. Suresh, B. Ramachandra Reddy, "Recovery of nickel and molybdate from ammoniacal leach liquors of spent HDS catalysts using chelating ion exchange resin," *Hydrometallurgy,* vol. 184, pp. 88-94, 2019.

[19] Chao Wang, Shubin Wang, Feng Yan, Zhen Zhang, Xuehua Shen, Zuotai Zhang, "Recycling of spent lithium-ion batteries: Selective ammonia leaching of valuable metals and simultaneous synthesis of high-purity manganese carbonat.," *Waste Management,* vol. 114, p. 253–262, 2020.

[20] CHEN Sheng-li(陈胜利), GUO Xue-yi(郭学益), SHI Wen-tang(石文堂), LI Dong(李栋), "Extraction of valuable metals from low-grade nickeliferous laterite ore by reduction roasting-ammonia leaching method," *J. Cent. South Univ. Technol,* p. 765−769, 2010.

[21] Y. Yang, K. Raipala, L. Holappa, "Ironmaking," *Treatise on Process Metallurgy,* vol. 3, pp. 2-88, 2014.

[22] "TATA Steel," 2013. [Online]. Available: https://www.tatasteeleurope.com/sites/default/files/1462%20TATA%20Hilan.pdf. [Accessed 2024].

[23] "TATA Steel," 2013. [Online]. Available: https://www.tatasteeleurope.com/sites/default/files/1462%20TATA%20Hilumin.pdf. [Accessed 2024].

[24] G. Dubpernell, "The story of Nickel plating," *Plating,* 1959.

[25] Dhaatri Resource Centre for Women and Children, 2016. [Online]. Available: https://view.officeapps.live.com/op/view.aspx?src=https%3A%2F%2Fwww.ohchr.org%2Fsites%2Fdefault%2Ffiles%2FDocuments%2FHRBodies%2FCRC%2FDiscussions%2F2016%2FDhaatri.docx%23%3A~%3Atext%3DThe%2520mining%2520industry%2520in%2520India%2Cto%2520domestic%2520and. [Accessed March 2024].

[26] “ILO,” 2019. [Online]. Available: https://www.ilo.org/wcmsp5/groups/public/---asia/---ro-bangkok/---ilo-manila/documents/publication/wcms_720743.pdf. [Accessed 29 March 2024].

[27] B. K. Sovacool, “When subterranean slavery supports sustainability transitions? power, patriarchy, and child labor in artisanal Congolese cobalt mining,” *The Extractive Industries and Society,* vol. 8, p. 271–293, 2021.

[28] C. Church and A. Crawford , “ISDD,” 2018. [Online]. Available: https://www.iisd.org/story/green-conflict-minerals/#group-Nickel-WSWW3nGCog. [Accessed 2024].

[29] European Commission, “European Commission,” European Commission, [Online]. Available: https://policy.trade.ec.europa.eu/development-and-sustainability/conflict-minerals-regulation_en#:~:text=In%20politically%20unstable%20areas%2C%20armed,mobile%20phones%2C%20cars%20and%20jewellery.. [Accessed April 2024].

[30] “Eurostat,” European Union, November 2023. [Online]. Available: https://ec.europa.eu/eurostat/web/products-eurostat-news/w/ddn-20231124-2. [Accessed April 2024].

[31] H. E. Melin, *The lithium-ion battery end-of-life market – A baseline study.*

[32] Megha Goyal , Kulwant Singh, Nitu Bhatnagar, “Circular economy conceptualization for lithium-ion batteries- material procurement and disposal process,” *Chemical Engineering Science,* vol. 281, 2023.

[33] Elsa Olivetti, Jeremy Gregory, Randolph Kirchain, “LIFE CYCLE IMPACTS OF ALKALINE BATTERIES WITH A FOCUS ON END-OF-LIFE,” THE NATIONAL ELECTRICAL MANUFACTURERS ASSOCIATION, 2010.

[34] Ramsey Hamadea, Raghid Al Ayache, Makram Bou Ghanem, Sleiman El Masri, Ali Ammouri, “Life Cycle Analysis of AA Alkaline Batteries,” *Procedia Manufacturing,* vol. 43, p. 415–422, 2020.

[35] J. Jandovi, M. Pedlik, “Leaching behaviour of iron-nickel alloys in ammoniacal solution,” *Hydrometalurgy,* vol. 35, pp. 123-128, 1994.

[36] L. J. M. López, “Brief history of the emergence of hydrometallurgical technology from the carbonate-ammoniacal leaching process of Ni and Co,” *Chemical Technology,* vol. 34, 2014.

[37] “Het Geheugen,” geheugen.delpher.nl, [Online]. Available: https://geheugen.delpher.nl/nl/geheugen/view?identifier=CBG01%3A3690. [Accessed September 2024].

[38] M. H. Caron, “Ammonia Leaching of Nickel and Cobalt Ores,” *TRANSACTIONS AIME,* vol. 188, 1950.

[39] XINGHUI MENG, and KENNETH N. HAN, “The Principles and Applications of Ammonia Leaching of Metals - A Review,” *Mineral Processing and Extractive Metallurgy Review,* vol. 16, no. 1, pp. 23-62, 2008.

[40] D. G. E. Kerfoot, “Nickel,” Ullmann's Encyclopedia of Industrial Chemistry, 2000.

[41] Junhong Zhang, Lihua Gao, Zhijun He, Xinmei Hou, Wenlong Zhan, Qinghai Pang, “Separation and recovery of iron and nickel from low-grade laterite nickel ore by microwave carbothermic reduction roasting,” *Journal of Materials Research and Technology,* vol. 9, pp. 12223-12235, 2022.

[42] Sadia Ilyas, Hyunjung Kim & Rajiv Ranjan Srivastava, “Carbothermic Reduction Roasting of a Low-Grade Nickel Laterite Ore in the Modified Caron Process,” in *Ni-Co 2021: The 5th International Symposium on Nickel and Cobalt*, 2021.

[43] Dongmin Li , Bao Zhang , Long Ye , Zhiming Xiao , Lei Ming , Xing Ou, “Regeneration of high-performance Li1.2Mn0.54Ni0.13Co0.13O2 cathode material from mixed spent lithium-ion batteries through selective ammonia leaching,” *Journal of Cleaner Production,* vol. 349, 2022.

[44] A. N. Nikoloski and M. Nicol, “The Electrochemistry of the Leaching Reactions in the Caron process II. Cathodic processes,” in *Conference: The 7th International Symposium on Electrochemistry in Mineral and Metal Processing*, Denver, Colorado, 2006.

[45] Abraham A.B. Araneda, Martin A. Rodriguez, Raul B. Rebak, Mariano A. Kappes, Ricardo M. Carranza, “Effect of thiosulfate on the pitting corrosion of nickel base alloys in chloride solutions,” in *Corrosion conference and expo,* 2017.

[46] Hosni Ezuber, Abdulla Alshater, and Moneer Abulhasan , “Role of thiosulfate in sucebtability of ASI 316L Austenitic stainless steels to pitting corrosion in 3.5% sodium cholride solutions.,” *Surface engineering and applied electrochemistry,* vol. 53, pp. 493-500, 2017.

[47] H.S. KIM, Y.T. KHO, K. OSSEO-ASARE, and H.W. PICKERING, “Active and Passive Behavior of Sintered Iron in Ammoniacal Ammonium Carbonate Solution,” *Metallurgical transactions,* vol. 22B, pp. 323-332, 1991.

[48] Jaesang Lee, Urs von Gunten, and Jae-Hong Kim, “Persulfate-Based Advanced Oxidation: Critical Assessment of Opportunities and Roadblocks,” *Environ. Sci. Technol.,* vol. 54, 2020.

[49] Tereza Evangelista and Sabrina Ferreira, “Sodium Persulfate (Na2S2O8),” *SynOpen,* vol. 5, pp. 291-293, 2021.

[50] “Lerochem,” Lerochem, [Online]. Available: https://lerochem.eu/en/pagrindinis/91-458-sodium-thiosulfate-pentahydrate-99-kg.html#/37-product_size_kg-1000_kg. [Accessed 2024].

[51] “Rheinperchemie,” Rheinperchemie, [Online]. Available: https://www.rheinperchemie.com/products/ammonium-persulfate. [Accessed 2024].

[52] “waternewseurope,” 2021. [Online]. Available: https://www.waternewseurope.com/water-prices-compared-in-36-eu-cities/. [Accessed 2024].

[53] “scrapmonster,” scrapmonster, 2024. [Online]. Available: https://www.scrapmonster.com/metal/steel-price/europe/300. [Accessed 2024].

[54] “index mundi,” index mundi , [Online]. Available: https://www.indexmundi.com/commodities/?commodity=nickel&currency=eur&months=60. [Accessed 2024].